Title

A Drosophila Tumor Suppressor Gene Prevents Tonic TNF Signaling through Receptor N-Glycosylation

Journal

Developmental Cell, 45(5)

ISSN

1534-5807

Authors

de Vreede, Geert
Morrison, Holly A
Houser, Alexandra M
et al.

Publication Date

2018-06-01

DOI

10.1016/j.devcel.2018.05.012

Peer reviewed

A Drosophila tumor suppressor gene prevents tonic TNF signaling through receptor N-glycosylation

Geert de Vreede[1], Holly A. Morrison[1], Alexandra M. Houser[1], Ryan M. Boileau[1, 2], Ditte Andersen[3], Julien Colombani[3] and David Bilder[1]

Affiliations:
[1] Department of Molecular and Cell Biology, University of California-Berkeley, Berkeley CA, 94720, USA

[2] Present address: The Eli and Edythe Broad Center of Regeneration Medicine and Stem Cell Research, Center for Reproductive Sciences, University of California, San Francisco, San Francisco, CA 94143, USA

[3] University Nice Sophia Antipolis, CNRS, Inserm, iBV, Nice 06108, France

Lead Contact: David Bilder, bilder@berkeley.edu

SUMMARY

Drosophila tumor suppressor genes (TSGs) have revealed molecular pathways that control tissue growth, but mechanisms that regulate mitogenic signaling are far from understood. Here we report that the Drosophila TSG *tumorous imaginal discs (tid),* whose phenotypes were previously attributed to mutations in a DnaJ-like chaperone, are in fact driven by the loss of the N-linked glycosylation pathway component ALG3. *tid/alg3* imaginal discs display tissue growth and architecture defects that share characteristics of both 'neoplastic' and 'hyperplastic' mutants. Tumorous growth is driven by inhibited Hippo signaling, induced by excess JNK activity. We show that ectopic JNK activation is caused by aberrant glycosylation of a single protein --the fly TNF receptor homolog-- which results in increased binding to the continually circulating TNF. Our results suggest that N-linked glycosylation sets the threshold of TNFR signaling by modifying ligand-receptor interactions, and that cells may alter this modification to respond appropriately to physiological cues.

INTRODUCTION

Tumorigenesis is ultimately driven by dysregulated cellular signaling that promotes unchecked proliferation (Hanahan and Weinberg, 2011). Proliferation-regulating signaling pathways in animals are therefore normally under tight control, to prevent aberrant growth. The primary mechanism of signaling regulation is limited availability of ligand, although levels of receptor can also be regulated, as can receptor availability on the plasma membrane or even its polarized localization. A full understanding of the mechanisms that limit mitogenic signaling is an important goal of both basic biology and cancer research.

Major insight into growth regulation has arisen from research in model organisms like *Drosophila melanogaster.* For instance, Drosophila studies revealed key steps of receptor tyrosine kinase signaling and uncovered the phenomenon of cell competition (Amoyel and Bach, 2014; Duffy and Perrimon, 1994; Shilo, 1992; Simpson, 1979; Simpson and Morata, 1981). Additional insight into growth regulatory mechanisms has come from the analysis of fly 'tumor suppressor genes' (TSGs) (Hariharan and Bilder, 2006; Richardson and Portela, 2017). Disruption of a single fly TSG is sufficient to cause overproliferation in epithelial organs of the larva called imaginal discs. Initial genetic screens identified several classes of fly TSGs. The 'neoplastic' TSGs -- *discs large, lethal giant larvae,* and *scribble* (Bilder and Perrimon, 2000; Schneiderman and Gateff, 1967; Stewart et al., 1972) — revealed an intimate link between cell polarity and cell proliferation control, a principle also relevant to human cancers. The 'hyperplastic' TSGs --including *hippo*, *warts*, and *salvador*—uncovered the novel Hippo (Hpo) signal transduction pathway that is now recognized as a conserved growth control mechanism (Harvey et al., 2003; Jia et al., 2003; Justice et al., 1995; Kango-Singh et al., 2002; Pantalacci et al., 2003; Tapon et al., 2002; Udan et al., 2003; Wu et al., 2003; Xu et al., 1995). Even less prominent Drosophila TSGs such as *lethal giant discs* have demonstrated important biological concepts (Buratovich and Bryant, 1995; Klein, 2003).

One classical Drosophila TSG that remains understudied is *tumorous imaginal discs (tid)* (Gateff, 1978; Löffler et al., 1990). Imaginal discs of *tid* homozygous larvae develop into overgrown masses (Kurzik-Dumke et al., 1995). Genetic mapping and cytogenetic analyses attributed this phenotype to loss of a conserved molecular chaperone of the DnaJ family (Kurzik-Dumke et al., 1995). Evidence for a tumor-suppressive role for a mammalian homolog, hTid-1, has been presented (Chen et al., 2009; Copeland et al., 2011; Kurzik-Dumke et al., 2008). However, the exact molecular mechanism through which *tid* could regulate cell and tissue proliferation remains mysterious.

We report here that the *tid* gene was cloned incorrectly. Aberrant cell proliferation in the Drosophila mutant arises not from disruptions to the DnaJ homolog, but rather to an adjacent gene that encodes the mannosyltransferase ALG3, involved in N-linked glycosylation. We show that overgrowth in *tid/ALG3* mutants is caused by mis-glycosylation of a single transmembrane protein, the Drosophila TNF receptor homolog Grindelwald, which results in downstream activation of Jun N-terminal kinase (JNK) and inactivation of the growth-suppressing Hpo pathway. Our results suggest that this post-translational modification modulates ligand-receptor affinity in the TNFR pathway and thus provides a regulatory mechanism setting a dynamic threshold for JNK mediated

stress signaling and growth control.

RESULTS

Tumorous phenotypes of *tid* mutants

The mutant phenotype of the classical Drosophila TSG *tumorous imaginal discs (tid)* was described in 1992 (Kurzik-Dumke et al., 1992). *Tid* was reported to encode a DnaJ-like molecular chaperone (Kurzik-Dumke et al., 1995), but has received little attention since, prompting a reinvestigation. To characterize the loss of function phenotype, we generated tid^1/tid^2 transheterozygous animals. As previously described, these mutants develop into 'giant' L3 larvae bearing imaginal disc tumors. The disc proliferation rate is slow, such that *tid* discs are initially smaller than discs from comparably aged WT larvae. However, mutant larvae delay puparium formation up to 11 days, during which growth continues. *tid* discs show clear organizational defects, displaying abnormal thickness and tissue folding; cells have altered shape and F-actin levels are elevated (**Fig. 1A,B, Suppl. Fig 1A,B**). Similar phenotypes are observed in *tid* hemizygous animals. We directly counted dissociated wing disc cells and found that prior to pupation, *tid* mutants contain almost double the amount of cells as WT (**Fig. 1C**). Although more limited than the ~5-fold increase of a neoplastic mutant (*dlg*) or the ~3-fold increase of a hyperplastic mutant (*wts*) (**Suppl. Fig. 1C-E**), the increase demonstrates that loss of *tid* indeed causes tumorigenic overgrowth. To assess proliferative capacity beyond the larval stage, we transplanted *tid* discs into the abdomens of WT adult hosts. As previously described (Kurzik-Dumke et al., 1992), tumors recovered from these hosts after 17 days are extremely overgrown and display a strong increase in architectural disorganization (**Fig. 1D,E**). The unchecked imaginal disc proliferation caused by *tid* mutations confirm that *tid* is a bona fide TSG.

tid displays characteristics of neoplastic and hyperplastic TSGs

To further investigate the mutant phenotype, we assessed mitotic clones. When homozygous *tid* eye discs in an otherwise heterozygous larva were generated, animals displayed the pupal lethal phenotype also seen when animals carry neoplastic TSG mutant eye discs (Menut et al., 2007). The eye discs display mild phenotypes compared to fully mutant animals (**Suppl. Fig. 1F-I**), suggesting that perdurance of the *tid* gene product or its substrates is too strong to effectively deplete using clonal strategies.

Unlike neoplastic mutants, apicobasal polarity markers showed no obvious disruption, although *tid* cells are more cuboidal than the columnar epithelium of WT or hyperplastic TSG mutant discs (**Suppl**. **Fig. 1J-L**). Other distinct properties of various TSG mutants include susceptibility to cell competition and cooperativity with oncogenes (Brumby and Richardson, 2003; Pagliarini, 2003). Clonal loss of neoplastic but not hyperplastic TSGs induces cell competition and elimination of the mutant cells; however, when combined with expression of oncogenic RasV12, neoplastic clones show dramatically synergistic overgrowth as well as tissue invasion. Using the MARCM system (Lee and Luo, 2001), we induced *tid* clones with or without RasV12 expression (**Fig. 1F-I**). *tid* clones were recovered but at an abundance lower than WT, indicating that they are partially outcompeted (**Suppl. Fig. 1M**). When *tid* clones also expressed RasV12, cooperative overgrowth was clearly observed, albeit less extreme than that

between *scrib* and RasV12 and lacking invasion (**Fig. 1I**). Thus, *tid* shares characteristics of both neoplastic and hyperplastic TSGs.

Tid mutants disrupt *CG4804*

The original sequencing analysis of the tid^1 and tid^2 alleles failed to identify molecular lesions within any protein coding sequence. These experiments did identify a lesion in the 5' UTR of the DnaJ-encoding *CG5504* in tid^2, leading to the suggestion that this lesion disrupted *CG5504* transcription (Kurzik-Dumke et al., 1995). However, the *CG5504* open reading frame (ORF) is found in the intron of a second ORF, *CG4084* (aka *neighbor of tid (l(2)not)* (**Fig. 2A**). Our sequencing of tid^1 and tid^2 identified lesions in the *CG4084* ORF in both alleles. tid^1 induces a nonsense mutation at glutamine 375, resulting in a truncation of the remaining 135 amino acids of the predicted CG4084 protein. In tid^2, we confirmed the previously reported molecular lesions: a 24 base pair deletion and a single base pair insertion. Within the *CG4084* ORF these lesions induce an in-frame deletion that removes amino acids 36-43, and a frameshift leading to premature termination of the protein after 192 amino acids (**Fig. 2A**). These data raise the possibility that loss of *CG4084* function, rather than *CG5504,* may in fact be responsible for the *tid* phenotype. To rigorously test this, we performed a rescue assay using constructs driving the *CG4084* ORF alone under either direct (*tubulin)* or UAS control. When these constructs were expressed in either tid^1 or tid^2 flies, they rescued lethality, as well as both the imaginal disc (**Fig. 2C,D**) and the pupal lethal phenotypes. We conclude that the *tid* gene was originally miscloned, and that the observed tumorous phenotype is actually due to loss of *CG4804* function.

CG4804 encodes *Drosophila* ALG3, and mutants show defective N-glycosylation

We next sought to identify the molecular function of *CG4084*. BLAST searches revealed that *CG4084* is the single fly homolog of the yeast and human *Asparagine-Linked Glycosylation-3 (ALG3)* genes. *ALG3* encodes a mannosyltransferase required for the biosynthesis of lipid-linked oligosaccharides in the endoplasmic reticulum (ER) N-glycosylation pathway, which is conserved from yeast to humans (**Fig. 2B**). To avoid confusion with the previous annotation, we will refer hereafter to the *CG4084* gene as *alg3*, and to the *tid1* and *tid2* alleles as mutations in *alg3*. To confirm that *alg3* mutants are defective in N-glycosylation, we turned to biochemical analysis of E-cadherin (Ecad), which has 4 N-glycosylation sites (**Fig. 2E**). In Western blots, Ecad from *alg3* discs runs at a lower molecular weight than in WT discs. Following treatment with Peptide-*N*-Glycosidase (PNGase), an enzyme that completely removes N-linked glycans, the band shift in *alg3* discs is increased and is equivalent to that in PNGase-treated WT discs (**Fig. 2E**). This demonstrates that *alg3* mutants have aberrant but not a complete lack of N-glycosylation, consistent with the role of Alg3 within the N-glycosylation pathway (**Fig. 2B**). Related phenotypes were observed with mutants in *alg9,* which acts immediately after *alg3* in the N-glycosylation pathway (**Suppl. Fig. 2A-E**). These data indicate that proper N-glycosylation is required for normal epithelial growth and architecture.

Hpo-dependent Yki activation in *alg3* mutants drives tumorous overgrowth

In order to determine how N-glycosylation ensures normal disc growth, we investigated mitogenic pathways that might be activated in *alg3* tumors. Reporters for STAT, Notch, and Wg signaling, pathways that drive disc overproliferation in other mutants (Bach et al., 2003; Classen et al., 2009; Moberg et al., 2005; Pellock et al., 2007; Thompson et al., 2005; Vaccari and Bilder, 2005), were largely normal in *alg3* discs (**Suppl. Fig. 3A-F**). Mispolarization of aPKC, a hallmark of neoplastic TSG mutants, was also not seen (**Suppl. Fig. 1K**), and reducing aPKC levels did not affect the *alg3* phenotype (**Suppl. Fig. 3G,H**). N-glycosylation aids protein maturation in the ER, and perturbation of this process can trigger the Unfolded Protein Response (UPR) (Davenport et al., 2008). A transgenic UPR reporter was strongly induced in *alg3* tissue, but inhibiting the UPR did not notably change their size or morphology (**Suppl. Fig. 3K-M**). Because both neoplastic and hyperplastic TSG mutants inhibit Hpo pathway kinases and induce pro- growth Yki activity (Menendez et al., 2010; Robinson and Moberg, 2011; Sun and Irvine, 2011), we investigated whether this pathway plays a role in *alg3* tumors. Interestingly, reporters for Yki activity were clearly upregulated in *alg3* as well as *alg9* mutant tissue (**Fig. 3A,B, Suppl. Fig. 2F-I**). We then reduced Yki activity, using overexpression of the inhibitory kinases Hpo and Wts under conditions that do not affect WT disc growth. These manipulations significantly reduced *alg3* tumor size, albeit without restoring defective disc morphology (**Fig. 3C-E**), suggesting that *alg3* mutant overgrowth is driven by altered Hpo pathway activity.

alg3 mutants inhibit Hpo pathway via excessive JNK signaling

To assess how defective N-glycosylation could reduce Hpo pathway kinase activity, we considered candidate Hpo regulators, focusing on those altered in both neoplastic and hyperplastic tumors. The transmembrane apical polarity regulator Crumbs (Crb) has been implicated in Hpo signaling in multiple tumor types (Hamaratoglu et al., 2009; Robinson et al., 2010). However, depletion of Crb failed to influence the *alg3* phenotype (**Suppl. Fig. 3I,J**). An alternative route by which Yki is activated is through the induction of the c-Jun N-terminal Kinase (JNK) pathway (Fernandez et al., 2011; Ohsawa et al., 2012; Robinson and Moberg, 2011; Sansores-Garcia et al., 2011; Sun and Irvine, 2011). Strikingly, a transgenic reporter for JNK signaling was strongly upregulated in *alg3* discs (**Fig. 3F,G**). Elevated JNK activation was confirmed by immunostaining for phosphorylated JNK, which was clearly increased compared to WT (**Fig. 3H,I**). To test the functional relevance of excessive JNK activity, we blocked signaling in one half of *alg3* discs with a dominant negative form of JNK. While this does not affect WT discs (**Suppl. Fig. 3N**), in *alg3* it resulted in a potent rescue of the phenotype (**Fig. 3J**). Blocking JNK signaling does not only inhibited tumorous overgrowth, it also restored local tissue architecture, reduced F-actin levels and negated the extended larval stages of *alg3* larvae. The data suggest that Hpo-regulated Yki activation in *alg3* mutant discs is caused by excessive JNK signaling.

Glycosylated TNFR drives JNK-dependent overgrowth

We next examined how the JNK signaling cascade could be triggered by aberrant N-glycosylation. Since N-glycosylation acts mainly on transmembrane and secreted proteins, one candidate route is through the Drosophila Tumor Necrosis Factor Receptor (TNFR). Remarkably, RNAi-mediated depletion of the major fly TNFR

(Flybase: *grindelwald, grnd* (Andersen et al., 2015)) in one half of *alg3* discs induced a strong reversion of the tumorous phenotype, resembling the reversion induced by dominant negative JNK (**Fig. 4A,B**). Rescue was also induced by overexpression of the Grnd extracellular domain, which acts in a dominant negative fashion in other contexts (**Suppl. Fig. 4B,C**) (Andersen et al., 2015). In accordance with a general role during defective N-glycosylation, RNAi depletion of *grnd* also rescued *alg9* mutant defects (**Suppl. Fig. 2C**). By contrast, depletion of a second Drosophila TNFR homolog (Flybase: *wengen* (Kanda et al., 2002)) did not rescue *alg3* tumors (**Fig. 4C**).

To determine whether Grnd could be a direct target of Alg3 function, we first assessed whether Grnd was N-glycosylated *in vivo*. Western blotting of Grnd in imaginal tissue showed a significant molecular weight reduction when extracts were treated with PNGase to remove N-linked glycans (**Fig. 4D,E, Suppl. Fig. 4A**). Grnd from *alg3* discs showed a higher molecular weight than from PNGase-treated WT discs, but this difference was eliminated when *alg3* discs were also treated with PNGase (**Fig. 4E, Suppl. Fig. 4A**). Analysis of Grnd protein sequence suggested a single high-confidence N-glycosylation site, at aspargine 63 (**Fig. 4F**). This site lies within the cysteine-rich domain (CRD) of Grnd, and close to the glycosphingolipid-binding motif (GBM), which are characteristic for TNFR family members. Consistent with this analysis, replacement of asparagine 63 with alanine in transgenic Grnd (GrndN63A) produced a protein running at a molecular weight identical to that of PNGase-treated WT Grnd (**Fig. 4D**), and this was not further altered by PNGase treatment. These results demonstrate that Grnd, which shows excessive signaling in *alg3* mutants, is normally glycosylated at N63.

Circulating TNF produced in the fat body activates TNFR

TNFR signaling is triggered by binding to the secreted ligand Tumor Necrosis Factor (TNF) (Brenner et al., 2015). Because the Drosophila genome encodes a single TNF homolog (Flybase: Eiger, Egr) (Igaki et al., 2002), we investigated the role of Egr in *alg3* mutants. Interestingly, depleting Egr in *alg3* discs did not result in any amelioration of the phenotype (**Fig. 5A,B**). This suggested that either TNFR hyperactivation in this context was ligand-independent, or that the TNF involved is produced in a separate, non-imaginal tissue. Consistent with the latter, ubiquitous depletion of Egr reverts the *alg3* tumor phenotype (**Fig. 5C**). One candidate source for Egr production is hemocytes, which are attracted to neoplastic tumors and locally secrete Egr (Bidla et al., 2007; Parisi et al., 2014; Pérez et al., 2017). However, hemocyte-specific depletion of Egr in *alg3* larvae also did not affect the tumor phenotype (**Suppl. Fig. 4D,E**), nor could we detect hemocyte attachment to *alg3* discs. An alternate source for Egr is the fat body (Agrawal et al., 2016; Mabery and Schneider, 2010). Strikingly, fat body-specific depletion of Egr in *alg3* larvae led to a strong rescue of the tumor phenotype (**Fig. 5D**), establishing that circulating Egr produced in a remote tissue activates Grnd in imaginal discs to trigger excessive JNK signaling.

Like Grnd, Egr is a glycoprotein (Kauppila et al., 2003), and thus could also be regulated by N-glycosylation. We used local expression of a *UAS-alg3* rescue construct to determine the tissue requirement for N-glycosylation in suppression of these JNK-driven tumors. Restoring Alg3 function to the fat body did not alter the *alg3* mutant phenotype, while restoring Alg3 function to imaginal discs clearly rescued the tissue

(**Fig. 5E,F**). This strongly suggests that while Egr is necessary for aberrant JNK activation in *alg3* mutants, its N-glycosylation does not play a role in the phenotype.

N-glycosylation reduces TNFR-TNF binding to regulate signaling

Given the evidence for a direct regulatory role of Grnd N-glycosylation, we examined whether N-glycosylation-deficient Grnd exhibits excess JNK signaling activity. Overexpression of GrndN63A in imaginal discs alone did not produce an evident phenotype, suggesting that any increase in JNK activity was low (**Suppl. Fig. 4F**). Similarly, overexpression of Egr in the fat body to elevate circulating levels of the ligand had no effect on WT discs (**Suppl. Fig. 4G**). However, elevation of circulating Egr induced a strong enhancement of the *alg3* phenotype, accompanied by increased JNK signaling and cell death (**Suppl. Fig. 4J,K, Fig. 6B',C'**). We also assayed an independent tissue in which Grnd is active. Egr- and Grnd-dependent JNK signaling is activated in the insulin-producing cells (IPCs) of the larval brain to limit overall growth of the animal in conditions when nutrient consumption is low (Agrawal et al., 2016). In line with these findings, overexpression of the Grnd intracellular domain in the IPCs, which induces ectopic JNK activation, reduces animal size, assayed by pupal volume (**Fig. 6K,L**). Interestingly, overexpression of GrndN63A in IPCs also resulted in a clear reduction of pupal volume, whereas overexpression of WT Grnd had no effect (**Fig. 6L**). Together these data indicate that preventing N-glycosylation of Grnd induces increased ligand sensitivity, to activate JNK.

How could N-glycosylation of Grnd enhance its signaling? Glycosylation can influence protein trafficking, but the WT apical localization of Grnd remains intact in *alg3* tumors (**Suppl. Fig. 4H,I**). In addition, GrndN63A remains apically localized and does not perturb disc architecture, arguing against changes in receptor or ligand accessibility (**Suppl. Fig. 4F,L,M**). Because the N-glycosylation site in Grnd is located in the predicted TNF-binding domain, an attractive alternative possibility is that N-glycosylation alters receptor-ligand affinity. To explore Egr-Grnd interactions, we expressed Venus-tagged Egr in the fat body and monitored its accumulation in the imaginal disc. While WT discs show little Egr association in this assay, *alg3* discs extensively accumulated Egr, despite the fact that Grnd levels are not increased (**Fig. 6A-C, Suppl. Fig 4N-Q**). This result suggests that impaired glycosylation could increase the affinity of Grnd for Egr. In an *ex vivo* system where Egr-Venus-expressing fat body is cultured alongside imaginal discs (**Fig. 6D**), cells that express transgenic Grnd bound significantly more Egr when they were mutant for *alg3* than when they were WT (**Fig. 6E-G**). An even stronger increase of bound Egr was seen in WT cells expressing GrndN63A, which is predicted to lack all N-glycans (**Fig. 6H-J**). Importantly, Grnd protein levels at the membrane remain comparable in both co-culture experiments, indicating that increased Egr binding is not simply caused by elevated receptor abundance (**Suppl. Fig. 4R,S**). These data suggest that physiological N-glycosylation regulates TNFR ligand binding, specifically by reducing its affinity for TNF.

DISCUSSION

We have shown that mutations in the classical Drosophila TSG *tumorous imaginal discs* (*tid*) disrupt the *ALG3* homolog *CG4084*, altering the lipid-linked biosynthetic pathway that generates oligosaccharides for protein N-linked glycosylation. Although altered glycosylation affects many proteins and can induce a UPR, we find that the growth control phenotype of *Alg3* can be ascribed to a single target and a single mechanism. This target is the Drosophila TNFR homolog, whose proper modification at a single extracellular site is required to prevent inappropriate TNF binding, subsequent JNK activation, and downstream Yki-driven overproliferation. We postulate that N-glycosylation can act as a mechanism to modulate JNK signaling in response to cellular stresses.

The *alg3* mutations studied here were originally identified for their overgrowth phenotype in imaginal discs (Kurzik-Dumke et al., 1992). Like most other Drosophila TSGs, this phenotype is caused by changes in Hpo-regulated Yki activation, but *alg3* mutants differ in both upstream regulation and downstream targets. Mutations in core Hpo signaling components result in rapid proliferation of disc cells, while the slow growth of *alg3* mutant tissue resembles that of the 'neoplastic' TSGs. Nonetheless, the STAT pathway, which is a major mitogenic effector in neoplastic mutants (Bunker et al., 2015; Gilbert et al., 2009; Wu et al., 2010), is not elevated in *alg3* tissue. Upstream, JNK-dependent Yki activity is seen in both *alg3* and neoplastic mutants (Menendez et al., 2010; Sun and Irvine, 2011). However, JNK activation in neoplastic mutants has been suggested to occur either through ligand-independent Grnd activation caused by alteration to apicobasal polarity (Andersen et al., 2015), or through Grnd-independent mechanisms (Muzzopappa et al., 2017). In *alg3* mutants, polarity is intact and overgrowth entirely relies on a Grnd-Egr axis, specifically the increased sensitivity of misglycosylated Grnd for endocrine Egr. Thus, TNFR signaling induced by altered N-glycosylation seems to define distinct consequences for downstream Hpo-mediated growth control.

While we have not tested biochemical affinities directly, our data are consistent with a model where TNF binding properties are directly regulated by glycosylation of TNFR. Partial or complete removal of the glycan at N63, within the ligand binding domain of Grnd, leads to an increase of bound Egr, indicating that N-glycosylation normally limits Grnd engagement and downstream signaling. In Drosophila larvae, Egr is continuously transcribed in the fat body for secretion into the hemolymph, bathing Grnd-expressing tissues including imaginal discs and IPCs in ligand (Agrawal et al., 2016). Our results suggest that proper N-glycosylation of Grnd sets a threshold that prevents tonic signaling in these and other tissues under normal circumstances. This raises the intriguing possibility that cell-autonomous changes in N-glycosylation, perhaps induced by stress inputs, could modulate ligand affinity, allowing a rapid and local response to this endocrine signal under different physiological conditions.

The modulation of Grnd ligand binding suggested here echoes the regulation of Notch by the glycosyltransferase Fringe (Stanley and Okajima, 2010; Takeuchi and Haltiwanger, 2014). However, the obligate role of Alg3 in all N-glycan synthesis is fundamentally distinct from Fringe's substrate-specific elaboration of a particular O-glycan. In the case of Notch, the specific sugar residues added by Fringe alter receptor

selectivity for one ligand over another (Brückner et al., 2000; Moloney et al., 2000). Since either aberrant or absent Grnd N-glycosylation results in increased ligand binding and ectopic signaling, evidence for specific glycan structures in modulating the ligand-receptor interface does not currently exist. Whether the glycan could provide a simple steric obstacle to ligand binding or may regulate it through more complex interactions will await structural studies.

Grnd shows strong homology to vertebrate TNFR family members in its extracellular TNF binding domain, although downstream signaling in the fly acts mainly through JNK (Andersen et al., 2015; Igaki et al., 2002), in contrast to mammalian homologs that also signal through NFκB, p38, and caspases (Dempsey et al., 2003). Amongst the 29 mammalian TNFR superfamily members, at least 7 have predicted N-glycosylation sites in their extracellular domains. Several of these sites have been studied, and their proposed roles vary from promoting signaling to inhibiting it or being functionally neutral (Charlier et al., 2010; Han et al., 2015; Klíma et al., 2009; Shatnyeva et al., 2011; Vaitaitis and Wagner, 2010). Our results motivate analyses of the receptors BCMA and DR4, which are closely related to Grnd and whose predicted N-glycosylation sites each lie in an analogous location within the ligand-binding domain (Andersen et al., 2015).

The data presented above, which highlight a new mechanism for restraining TNF signaling, hint at pathogenic mechanisms for several human diseases. Altered glycosylation is emerging as a frequent hallmark of cancer, in which JNK signaling is increasingly implicated (Bubici and Papa, 2014; Pinho and Reis, 2015; Vajaria and Patel, 2017). Moreover, mutations in the extracellular domain of human TNFR1, including predicted N-glycosylation sites, can cause the autoinflammatory disease TRAPS (Tumour necrosis factor Receptor-Associated Periodic Syndrome) (Cantarini et al., 2012). Because the erroneous activation of Grnd in *alg3* mutants is akin to an autoinflammatory response, defective N-glycosylation could be an additional mechanism for hyperactive TNFR1 signaling. Finally, mutations in N-glycosylation pathway enzymes including Alg3 result in recessive genetic diseases called type I Congenital Disorders of Glycosylation (CDG-I) (Jaeken, 2012; Scott et al., 2014). CDG patients exhibit a variety of poorly characterized symptoms associated with multiple organs, and the etiology of CDG is largely unknown. Our finding of altered inflammatory TNFR/JNK signaling in analogous fly mutants provides a new avenue to investigate.

ACKNOWLEDGMENTS

We would like to thank U. Kurzik-Dumke, P. Leopold, G. Davis, I. Hariharan, A. Bergmann, J. Jiang, H. Ryoo and L. O'Brien for kindly providing reagents and K. Ten Hagen, M. Mapelli and C. Bertozzi for sharing expertise. We are grateful to J. Zeitler for help with antibody production, M. Bogaczynska for help with cell counts and the Bilder lab for discussions and manuscript comments. This work was supported by grants from the NIH (RO1 GM090150) and the Mizutani Institute for Glycoscience.

AUTHOR CONTRIBUTIONS

Conceptualization and Methodology, G.d.V., H.A.M. and D.B.; Investigation, G.d.V., H.A.M., A.M.H. and R.M.B.; Resources, J.C, D.A. and R.M.B.; Writing – Original Draft,

G.d.V. and D.B.

DECLARATION OF INTERESTS

The authors declare no competing interests.

REFERENCES

Agrawal, N., Delanoue, R., Mauri, A., Basco, D., Pasco, M., Thorens, B., and Léopold, P. (2016). The Drosophila TNF Eiger Is an Adipokine that Acts on Insulin-Producing Cells to Mediate Nutrient Response. Cell Metab. *23*, 675–684.

Amoyel, M., and Bach, E.A. (2014). Cell competition: how to eliminate your neighbours. Development *141*, 988–1000.

Andersen, D.S., Colombani, J., Palmerini, V., Chakrabandhu, K., Boone, E., Röthlisberger, M., Toggweiler, J., Basler, K., Mapelli, M., Hueber, A.-O., et al. (2015). The Drosophila TNF receptor Grindelwald couples loss of cell polarity and neoplastic growth. Nature *522*, 482–486.

Bach, E.A., Vincent, S., Zeidler, M.P., and Perrimon, N. (2003). A Sensitized Genetic Screen to Identify Novel Regulators and Components of the Drosophila Janus Kinase/Signal Transducer and Activator of Transcription Pathway. Genetics *165*, 1149–1166.

Bach, E.A., Ekas, L.A., Ayala-Camargo, A., Flaherty, M.S., Lee, H., Perrimon, N., and Baeg, G.H. (2007). GFP reporters detect the activation of the Drosophila JAK/STAT pathway in vivo. Gene Expr. Patterns *7*, 323–331.

Bidla, G., Dushay, M.S., and Theopold, U. (2007). Crystal cell rupture after injury in Drosophila requires the JNK pathway, small GTPases and the TNF homolog Eiger. J. Cell Sci. *120*, 1209–1215.

Bilder, D., and Perrimon, N. (2000). Localization of apical epithelial determinants by the basolateral PDZ protein Scribble. Nature *403*, 676–680.

Boedigheimer, M., and Laughon, a (1993). Expanded: a gene involved in the control of cell proliferation in imaginal discs. Development *118*, 1291–1301.

Brenner, D., Blaser, H., and Mak, T.W. (2015). Regulation of tumour necrosis factor signalling: live or let die. Nat. Rev. Immunol. *15*, 362–374.

Brückner, K., Perez, L., Clausen, H., and Cohen, S. (2000). Glycosyltransferase activity of Fringe modulates Notch-Delta interactions. Nature *406*, 411–415.

Brumby, A.M., and Richardson, H.E. (2003). scribble mutants cooperate with oncogenic Ras or Notch to cause neoplastic overgrowth in Drosophila. EMBO J. *22*, 5769–5779.

Bubici, C., and Papa, S. (2014). JNK signalling in cancer: In need of new, smarter therapeutic targets. Br. J. Pharmacol. *171*, 24–37.

Bunker, B.D., Nellimoottil, T.T., Boileau, R.M., Classen, A.K., and Bilder, D. (2015). The transcriptional response to tumorigenic polarity loss in Drosophila. Elife *2015*.

Buratovich, M. a, and Bryant, P.J. (1995). Duplication of l(2)gd imaginal discs in Drosophila is mediated by ectopic expression of wg and dpp. Dev. Biol. *168*, 452–463.

Cantarini, L., Lucherini, O.M., Muscari, I., Frediani, B., Galeazzi, M., Brizi, M.G., Simonini, G., and Cimaz, R. (2012). Tumour necrosis factor receptor-associated periodic syndrome (TRAPS): State of the art and future perspectives. Autoimmun. Rev. *12*, 38–43.

Charlier, E., Condé, C., Zhang, J., Deneubourg, L., Di Valentin, E., Rahmouni, S., Chariot, A., Agostinis, P., Pang, P.-C., Haslam, S.M., et al. (2010). SHIP-1 inhibits CD95/APO-1/Fas-induced apoptosis in primary T lymphocytes and T leukemic cells by promoting CD95 glycosylation independently of its phosphatase activity. Leukemia *24*, 821–832.

Chatterjee, N., and Bohmann, D. (2012). A versatile φC31 based reporter system for measuring AP-1 and NRF2 signaling in Drosophila and in tissue culture. PLoS One *7*.

Chen, C.Y., Chiou, S.H., Huang, C.Y., Jan, C.I., Lin, S.C., Hu, W.Y., Chou, S.H., Liu, C.J., and Lo, J.F. (2009). Tid1 functions as a tumour suppressor in head and neck squamous cell carcinoma. J Pathol *219*, 347–355.

Classen, A.K., Bunker, B.D., Harvey, K.F., Vaccari, T., and Bilder, D. (2009). A tumor suppressor activity of Drosophila Polycomb genes mediated by JAK-STAT signaling. Nat. Genet. *41*, 1150–1155.

Copeland, E., Balgobin, S., Lee, C.M., and Rozakis-Adcock, M. (2011). hTID-1 defines a novel regulator of c-Met Receptor signaling in renal cell carcinomas. Oncogene *30*, 2252–2263.

Davenport, E.L., Morgan, G.J., and Davies, F.E. (2008). Untangling the unfolded protein response. Cell Cycle *7*, 865–869.

Dempsey, P.W., Doyle, S.E., He, J.Q., and Cheng, G. (2003). The signaling adaptors and pathways activated by TNF superfamily. Cytokine Growth Factor Rev. *14*, 193–209.

Duffy, J.B., and Perrimon, N. (1994). The torso pathway in Drosophila: lessons on receptor tyrosine kinase signaling and pattern formation. Dev. Biol. *166*, 380–395.

Fernandez, B.G., Gaspar, P., Bras-Pereira, C., Jezowska, B., Rebelo, S.R., and Janody, F. (2011). Actin-Capping Protein and the Hippo pathway regulate F-actin and tissue growth in Drosophila. Development *138*, 2337–2346.

Gateff, E. (1978). Malignant neoplasms of genetic origin in Drosophila melanogaster. Science (80-.). *200*, 1448–1459.

Gilbert, M.M., Beam, C.K., Robinson, B.S., and Moberg, K.H. (2009). Genetic interactions between the Drosophila tumor suppressor gene ept and the stat92E transcription factor. PLoS One *4*.

Hamaratoglu, F., Gajewski, K., Sansores-Garcia, L., Morrison, C., Tao, C., and Halder, G. (2009). The Hippo tumor-suppressor pathway regulates apical-domain size in parallel to tissue growth. J. Cell Sci. *122*, 2351–2359.

Han, L., Zhang, D., Tao, T., Sun, X., Liu, X., Zhu, G., Xu, Z., Zhu, L., Zhang, Y., Liu, W.,

et al. (2015). The role of N-Glycan modification of TNFR1 in inflammatory microglia activation. Glycoconj. J. *32*, 685–693.

Hanahan, D., and Weinberg, R.A. (2011). Hallmarks of cancer: the next generation. Cell *144*, 646–674.

Hariharan, I.K., and Bilder, D. (2006). Regulation of Imaginal Disc Growth by Tumor-Suppressor Genes in Drosophila. Annu. Rev. Genet *40*, 335–361.

Harvey, K.F., Pfleger, C.M., and Hariharan, I.K. (2003). The Drosophila Mst ortholog, hippo, restricts growth and cell proliferation and promotes apoptosis. Cell *114*, 457–467.

Igaki, T., Kanda, H., Yamamoto-Goto, Y., Kanuka, H., Kuranaga, E., Aigaki, T., and Miura, M. (2002). Eiger, a TNF superfamily ligand that triggers the Drosophila JNK pathway. EMBO J. *21*, 3009–3018.

Jaeken, J. (2012). Congenital disorders of glycosylation. In Inborn Metabolic Diseases: Diagnosis and Treatment, pp. 607–616.

Jia, J., Zhang, W., Wang, B., Trinko, R., and Jiang, J. (2003). The Drosophila Ste20 family kinase dMST functions as a tumor suppressor by restricting cell proliferation and promoting apoptosis. Genes Dev. *17*, 2514–2519.

Justice, R.W., Zilian, O., Woods, D.F., Noll, M., and Bryant, P.J. (1995). The Drosophila tumor suppressor gene warts encodes a homolog of human myotonic dystrophy kinase and is required for the control of cell shape and proliferation. Genes Dev. *9*, 534–546.

Kanda, H., Igaki, T., Kanuka, H., Yagi, T., and Miura, M. (2002). Wengen, a member of the Drosophila tumor necrosis factor receptor superfamily, is required for eiger signaling. J. Biol. Chem. *277*, 28372–28375.

Kango-Singh, M., Nolo, R., Tao, C., Verstreken, P., Hiesinger, P.R., Bellen, H.J., and Halder, G. (2002). Shar-pei promotes proliferation arrest during imaginal disc growth in Drosophila. Development *129*, 5719–5730.

Kauppila, S., Maaty, W.S.A., Chen, P., Tomar, R.S., Eby, M.T., Chapo, J., Chew, S., Rathore, N., Zachariah, S., Sinha, S.K., et al. (2003). Eiger and its receptor, Wengen, comprise a TNF-like system in Drosophila. Oncogene *22*, 4860–4867.

Keller, L.C., Cheng, L., Locke, C.J., Müller, M., Fetter, R.D., and Davis, G.W. (2011). Glial-derived prodegenerative signaling in the drosophila neuromuscular system. Neuron *72*, 760–775.

Klein, T. (2003). The tumour suppressor gene l(2)giant discs is required to restrictthe activity of Notch to the dorsoventral boundary during Drosophila wing development. Dev. Biol. *255*, 313–333.

Klíma, M., Zájedová, J., Doubravská, L., and Anděra, L. (2009). Functional analysis of the posttranslational modifications of the death receptor 6. Biochim. Biophys. Acta - Mol. Cell Res. *1793*, 1579–1587.

Kurzik-Dumke, U., Phannavong, B., Gundacker, D., and Gateff, E. (1992). Genetic, cytogenetic and developmental analysis of the Drosophila melanogaster tumor suppressor gene lethal(2)tumorous imaginal discs (1(2)tid). Differentiation. *51*, 91–104.

Kurzik-Dumke, U., Gundacker, D., Renthrop, M., and Gateff, E. (1995). Tumor suppression in Drosophila is causally related to the function of the lethal(2) tumorous imaginal discs gene, a dnaJ homolog. Dev. Genet. *16*, 64–76.

Kurzik-Dumke, U., Hörner, M., Czaja, J., Nicotra, M.R., Simiantonaki, N., Koslowski, M., and Natali, P.G. (2008). Progression of colorectal cancers correlates with overexpression and loss of polarization of expression of the htid-1 tumor suppressor. Int. J. Mol. Med. *21*, 19–31.

Lee, T., and Luo, L. (2001). Mosaic analysis with a repressible cell marker (MARCM) for Drosophila neural development. Trends Neurosci. *24*, 251–254.

Liu, F., and Posakony, J.W. (2014). An enhancer composed of interlocking submodules controls transcriptional autoregulation of suppressor of hairless. Dev. Cell *29*, 88–101.

Löffler, T., Wismar, J., Sass, H., Miyamoto, T., Becker, G., Konrad, L., Blondeau, M., Protin, U., Kaiser, S., and Gräf, P. (1990). Genetic and molecular analysis of six tumor suppressor genes in Drosophila melanogaster. Environ. Health Perspect. *88*, 157–161.

Mabery, E.M., and Schneider, D.S. (2010). The drosophila TNF ortholog eiger is required in the fat body for a robust immune response. J. Innate Immun. *2*, 371–378.

Mendoza-Topaz, C., Urra, F., Barria, R., Albornoz, V., Ugalde, D., Thomas, U., Gundelfinger, E.D., Delgado, R., Kukuljan, M., Sanxaridis, P.D., et al. (2008). DLGS97/SAP97 Is Developmentally Upregulated and Is Required for Complex Adult Behaviors and Synapse Morphology and Function. J. Neurosci. *28*, 304–314.

Menendez, J., Perez-Garijo, A., Calleja, M., and Morata, G. (2010). A tumor-suppressing mechanism in Drosophila involving cell competition and the Hippo pathway. Proc. Natl. Acad. Sci. *107*, 14651–14656.

Menut, L., Vaccari, T., Dionne, H., Hill, J., Wu, G., and Bilder, D. (2007). A mosaic genetic screen for Drosophila neoplastic tumor suppressor genes based on defective pupation. Genetics *177*, 1667–1677.

Moberg, K.H., Schelble, S., Burdick, S.K., and Hariharan, I.K. (2005). Mutations in erupted, the Drosophila ortholog of mammalian tumor susceptibility gene 101, elicit non-cell-autonomous overgrowth. Dev. Cell *9*, 699–710.

Moloney, D.J., Panin, V.M., Johnston, S.H., Chen, J., Shao, L., Wilson, R., Wang, Y., Stanley, P., Irvine, K.D., Haltiwanger, R.S., et al. (2000). Fringe is a glycosyltransferase that modifies Notch. Nature *406*, 369–375.

Muzzopappa, M., Murcia, L., and Milán, M. (2017). Feedback amplification loop drives malignant growth in epithelial tissues. Proc. Natl. Acad. Sci. 201701791.

Ohsawa, S., Sato, Y., Enomoto, M., Nakamura, M., Betsumiya, A., and Igaki, T. (2012). Mitochondrial defect drives non-autonomous tumour progression through Hippo signalling in Drosophila. Nature 10–15.

Pagliarini, R.A. (2003). A Genetic Screen in Drosophila for Metastatic Behavior. Science (80-.). *302*, 1227–1231.

Pantalacci, S., Tapon, N., and Léopold, P. (2003). The Salvador partner Hippo

promotes apoptosis and cell-cycle exit in Drosophila. Nat. Cell Biol. *5*, 921–927.

Parisi, F., Stefanatos, R.K., Strathdee, K., Yu, Y., and Vidal, M. (2014). Transformed epithelia trigger non-tissue-autonomous tumor suppressor response by adipocytes via activation of toll and eiger/TNF signaling. Cell Rep. *6*, 855–867.

Pellock, B.J., Buff, E., White, K., and Hariharan, I.K. (2007). The Drosophila tumor suppressors Expanded and Merlin differentially regulate cell cycle exit, apoptosis, and Wingless signaling. Dev. Biol. *304*, 102–115.

Pérez, E., Lindblad, J.L., and Bergmann, A. (2017). Tumor-promoting function of apoptotic caspases by an amplification loop involving ROS, macrophages and JNK in Drosophila. Elife *6*.

Pinho, S.S., and Reis, C.A. (2015). Glycosylation in cancer: mechanisms and clinical implications. Nat. Rev. Cancer *15*, 540–555.

Richardson, H.E., and Portela, M. (2017). Tissue growth and tumorigenesis in Drosophila: cell polarity and the Hippo pathway. Curr. Opin. Cell Biol. *48*, 1–9.

Robinson, B.S., and Moberg, K.H. (2011). Drosophila endocytic neoplastic tumor suppressor genes regulate Sav/Wts/Hpo signaling and the c-Jun N-terminal kinase pathwa. Cell Cycle *10*, 4110–4118.

Robinson, B.S., Huang, J., Hong, Y., and Moberg, K.H. (2010). Crumbs Regulates Salvador/Warts/Hippo Signaling in Drosophila via the FERM-Domain Protein Expanded. Curr. Biol. *20*, 582–590.

Ryoo, H.D., Li, J., and Kang, M.J. (2013). Drosophila XBP1 Expression Reporter Marks Cells under Endoplasmic Reticulum Stress and with High Protein Secretory Load. PLoS One *8*.

Sansores-Garcia, L., Bossuyt, W., Wada, K.I., Yonemura, S., Tao, C., Sasaki, H., and Halder, G. (2011). Modulating F-actin organization induces organ growth by affecting the Hippo pathway. EMBO J. *30*, 2325–2335.

Schindelin, J., Arganda-Carreras, I., Frise, E., Kaynig, V., Longair, M., Pietzsch, T., Preibisch, S., Rueden, C., Saalfeld, S., Schmid, B., et al. (2012). Fiji: an open-source platform for biological-image analysis. Nat. Methods *9*, 676–682.

Schneiderman, H.A., and Gateff, E. (1967). Developmental studies of a new mutant of Drosophila melanogaster: Lethal malignant brain tumor (l(2)gl 4). 7: 760.

Scott, K., Gadomski, T., Kozicz, T., and Morava, E. (2014). Congenital disorders of glycosylation: New defects and still counting. J. Inherit. Metab. Dis. *37*, 609–617.

Shatnyeva, O.M., Kubarenko, A. V., Weber, C.E.M., Pappa, A., Schwartz-Albiez, R., Weber, A.N.R., Krammer, P.H., and Lavrik, I.N. (2011). Modulation of the CD95-induced apoptosis: The role of CD95 N-glycosylation. PLoS One *6*.

Shilo, B.Z. (1992). Roles of receptor tyrosine kinases in Drosophila development. FASEB J. *6*, 2915–2922.

Simpson, P. (1979). Parameters of cell competition in the compartments of the wing disc of Drosophila. Dev. Biol. *69*, 182–193.

Simpson, P., and Morata, G. (1981). Differential mitotic rates and patterns of growth in compartments in the Drosophila wing. Dev. Biol. *85*, 299–308.

Stanley, P., and Okajima, T. (2010). Roles of glycosylation in notch signaling.

Stewart, M., Murphy, C., and Fristrom, J.W. (1972). The recovery and preliminary characterization of X chromosome mutants affecting imaginal discs ofDrosophila melanogaster. Dev. Biol. *27*, 71–83.

Sun, G., and Irvine, K.D. (2011). Regulation of Hippo signaling by Jun kinase signaling during compensatory cell proliferation and regeneration, and in neoplastic tumors. Dev. Biol. *350*, 139–151.

Takeuchi, H., and Haltiwanger, R.S. (2014). Significance of glycosylation in Notch signaling. Biochem. Biophys. Res. Commun. *453*, 235–242.

Tao, W., Zhang, S., Turenchalk, G.S., Stewart, R.A., St John, M.A., Chen, W., and Xu, T. (1999). Human homologue of the Drosophila melanogaster lats tumour suppressor modulates CDC2 activity. Nat. Genet. *21*, 177–181.

Tapon, N., Harvey, K.F., Bell, D.W., Wahrer, D.C.R., Schiripo, T.A., Haber, D.A., and Hariharan, I.K. (2002). salvador promotes both cell cycle exit and apoptosis in Drosophila and is mutated in human cancer cell lines. Cell *110*, 467–478.

Thompson, B.J., Mathieu, J., Sung, H.H., Loeser, E., Rørth, P., and Cohen, S.M. (2005). Tumor suppressor properties of the ESCRT-II complex component Vps25 in Drosophila. Dev. Cell *9*, 711–720.

Udan, R.S., Kango-Singh, M., Nolo, R., Tao, C., and Halder, G. (2003). Hippo promotes proliferation arrest and apoptosis in the Salvador/Warts pathway. Nat. Cell Biol. *5*, 914–920.

Uemura, T., Oda, H., Kraut, R., Hayashi, S., Kotaoka, Y., and Takeichi, M. (1996). Zygotic Drosophila E-cadherin expression is required for processes of dynamic epithelial cell rearrangement in the Drosophila embryo. Genes Dev. *10*, 659–671.

Vaccari, T., and Bilder, D. (2005). The Drosophila tumor suppressor vps25 prevents nonautonomous overproliferation by tegulating Notch trafficking. Dev. Cell *9*, 687–698.

Vaitaitis, G.M., and Wagner, D.H. (2010). CD40 glycoforms and TNF-receptors 1 and 2 in the formation of CD40 receptor(s) in autoimmunity. Mol. Immunol. *47*, 2303–2313.

Vajaria, B.N., and Patel, P.S. (2017). Glycosylation: a hallmark of cancer? Glycoconj. J. *34*, 147–156.

Wu, M., Pastor-Pareja, J.C., and Xu, T. (2010). Interaction between RasV12 and scribbled clones induces tumour growth and invasion. Nature *463*, 545–548.

Wu, S., Huang, J., Dong, J., and Pan, D. (2003). hippo encodes a Ste-20 family protein kinase that restricts cell proliferation and promotes apoptosis in conjunction with salvador and warts. Cell *114*, 445–456.

Wu, S., Liu, Y., Zheng, Y., Dong, J., and Pan, D. (2008). The TEAD/TEF family protein Scalloped mediates transcriptional output of the Hippo growth-regulatory pathway. Dev. Cell *14*, 388–398.

Xu, T., Wang, W., Zhang, S., Stewart, R.A., and Yu, W. (1995). Identifying tumor suppressors in genetic mosaics: the Drosophila lats gene encodes a putative protein kinase. Development *121*, 1053–1063.

Zhang, L., Ren, F., Zhang, Q., Chen, Y., Wang, B., and Jiang, J. (2008). The TEAD/TEF family of transcription factor Scalloped mediates Hippo signaling in organ size control. Dev. Cell *14*, 377–387.

FIGURE LEGENDS

Figure 1. *Tid* is a tumor suppressor.
Compared to WT (**A**), *tid* mutant wing imaginal discs (**B**) show disorganized tissue architecture and moderate overgrowth, quantified in (**C**). When *tid* tumors from a 10-day old larva are transplanted into the abdomen of an adult host (**D**) they continue proliferating and overgrow dramatically, with more severe architectural defects (**E**). (**F-G**) *tid* clones in the eye disc are partially outcompeted compared to WT. (**H,I**) *tid* mutations cooperate with RasV12 to strongly enhance overgrowth. ***P <0.001; Error bars indicate s.d. Images are representative of n≥10 animals per genotype. Scale bars: 100 μm in A, B, D and F; 10 μm in A'. See also **Figure S1**.

Figure 2. *Tid* mutants disrupt *CG4804*, encoding Drosophila ALG3
(**A**) Schematic displaying the location of tid^1 and tid^2 lesions, both lying within the *CG4804* ORF. (**B**) Steps of lipid-linked oligosaccharide synthesis in the N-linked glycosylation pathway. ALG3 is the first mannosyltransferase that acts within the ER lumen. After sequential addition of mannose and glucose monomers, the core glycan is transferred to the target protein, which is transported to the plasma membrane after further glycan trimming and modification within the Golgi. (**C,D**) Ubiquitous expression of *CG4804* rescues the *tid* tumorous phenotype. (**E**) E-cadherin Western Blots reveal a mobility shift in *alg3* mutants relative to WT. PNGase treatment of E-cadherin generates equivalent shifts in both genotypes, indicating a partial glycosylation defect in *alg3.* Images are representative of n≥10 animals per genotype. Scale bar: 100 μm in C. See also **Figure S2.**

Figure 3. Hippo and JNK drive the *alg3* phenotype
(**A,B**) The Hippo pathway reporter HREGFP is elevated in *alg3* discs compared to WT. (**C**) Reducing Hpo growth signaling through Wts or Hpo overexpression shows a robust tumor size reduction. *alg3-bx>* n=28 discs, *alg3-bx>wts* n=31 discs, *alg3-bx>hpo* n=24 discs. (**D,E**) Expressing Wts in *alg3* discs rescues tumorous overgrowth, though not architecture defects. The JNK pathway reporters AP1GFP (**F**) and pJNK (**H**) are elevated in *alg3* discs (**G,I**). (**J**) Blocking JNK signaling in the posterior half of *alg3* discs reduces overgrowth and restores tissue architecture. ***P<0.001; **P<0.01; Error bars indicate s.d. Images are representative of n≥10 animals per genotype. Scale bars: 100 μm in A, B and D; 10 μm in A'', B'' and J'. See also **Figures S2** and **S3.**

Figure 4. Glycoprotein Grnd/TNFR activates JNK signaling in *alg3*

(**A,B**) Knockdown of Grnd in the posterior half of *alg3* discs rescues overgrowth and tissue architecture. (**C**) Knockdown of Wgn does not rescue *alg3*. (**D**) Western Blotting of V5-tagged transgenic Grnd. Grnd N63A shows altered mobility on Western Blot corresponding to PNGase-treated WT Grnd. (**E**) Western Blotting with an antibody for endogenous Grnd in *alg3* shows a mobility shift compared to WT, and PNGase treatment causes equivalent shifts of both genotypes. Note the loading disparity in the fourth lane, and see **Supp. Fig. 4A** for quantitation. (**F**) The Grnd-ECD contains a single high-confidence predicted glycosylation site at N63 (NetNGlyc). CRD= cysteine-rich domain; GBM= glycosphingolipid-binding motif. Images are representative of n≥15 animals per genotype. Scale bar: 100 μm in A. See also **Figures S2** and **S4**.

Figure 5. Systemic Egr/TNFα produced by the fat body activates Grnd/TNFR in the wing disc

(**A,B**) Local RNAi depletion of Egr in the wing imaginal disc does not rescue *alg3* discs. (**C**) Ubiquitous knockdown of Egr rescues *alg3* discs, and depletion in the fat body (**D**) recapitulates that phenotype. (**E**) Driving *alg3* expression in the fat body does not rescue *alg3* discs, while (**F**) local expression within discs rescues overgrowth and architecture defects. Images are representative of n≥10 animals per genotype. Scale bar: 100 μm in A. See also **Figure S4**.

Figure 6. Grnd N-glycosylation reduces ligand binding

(**A**) Schematic representation of the experiments in (**B,C**): Venus-tagged Egr is expressed in the fat body of WT or *alg3* larvae. Egr-Venus binding and cell death (DCP-1) are elevated in *alg3* compared to WT. (**D**) Schematic representation of *ex vivo* co-culture using Egr-Venus expressing fat body tissue. When WT (**E**) and *alg3* (**F**) discs expressing Grnd in the posterior compartment are co-cultured, Egr-Venus binds more strongly to *alg3*: quantified in (**G**), *hh>grnd-HA WT* n=26 discs, *hh>grnd-HA alg3* n=30 discs. When discs expressing WT Grnd (**H**) and Grnd-N63A (**I**) are co-cultured, Egr-Venus binds more strongly to Grnd-N63A: quantified in (**J**), *hh>grnd-WT-V5* n=33 discs, *hh>grnd-N63A-V5* n=46 discs. (**K**) Circulating Egr binds Grnd on IPCs in the larval brain, activating JNK to inhibit pupal growth. (**L**) Changes in pupal volume caused by expression of Grnd constructs in IPCs. Grnd-N63A inhibits growth analogous to the dominant-active Grnd ICD. *dilp2>GFP* n=97, *dilp2>grnd KD* n=61, *dilp2>grnd ICD* n=64, *dilp2>grnd N63A* n=75*, dilp2>grnd WT* n=68. ***P <0.001; **P<0.01; *P<0.05; n.s., not significant; Error bars indicate s.e.m. Images are representative of n≥15 animals per genotype. Scale bar: 100 μm in B. See also **Figure S4**.

STAR METHODS

★ Contact for reagent and resource sharing

Further information and requests for resources and reagents should be directed to and will be fulfilled by the Lead Contact, David Bilder (bilder@berkeley.edu).

★ Experimental Model and Subject Details

Drosophila stocks and genetics

Drosophila melanogaster stocks were kept on cornmeal molasses food at room temperature and experimental crosses were raised at 25°C. *OreR* flies were used for WT controls. *alg*3^{tid1} *FRT42, alg*3^{tid2} *Kr FRT42* and *alg*3^{tid2} *FRT42* were used to generate transheterozygous animals, mitotic clones and transgenic recombinants. Other alleles and their sources are listed in the **Key Resources Table**. For imaginal disc samples third instar stage larvae were used. Since these larval imaginal discs are not sexually dimorphic, male and female samples were grouped together.

★ Method Details

Generating transgenic lines

The *l(2)not* coding sequence was amplified from cDNA FI07241 (BDGP). Amplicons were gel purified and ligated into pUASTB (Addgene). Grnd cDNA (P. Leopold) was subcloned and ligated into pBSkII. An oligo containing V5-STOPSTOP was created using this primer and its complement: AAAAACTCGAGGGCGGCGGCAAGCCCATC CCCAACCCCCTGCTGGGCCTGGATAGCACCTAATAATCTAGAAAAAA. pBSkII-Grnd and this oligo were cut and ligated together to create Grnd-V5. Using this Grnd-V5 construct, a quick-change mutagenesis was performed using CGAGGTCTGCAATG CCCAAACCCACAAC and its complement to create Grnd-N63A-V5. Grnd-V5 and Grnd-N63A-V5 were ligated into pUASTB. All constructs were sequence verified and targeted into either the *attP2* or *attP40* landing sites through embryo injections performed by BestGene, Inc.

Sequencing *tid* alleles

Genomic DNA was isolated from 50 hemizygous larvae using the 30 Fly Prep protocol (BDGP). The *tid/not* genomic region was amplified with Phusion high fidelity DNA polymerase (NEB) using the following primers: 5'-TTAATTTTCGCCGGTTATCA-3' (*l(2)not*-F) and 5'-ACTCAGACCATTTTACTGCA-3' (*l(2)not*-R). Amplicons were gel-purified and sequenced. Sequence data were aligned and analyzed using ContigExpress (Vector NTI); sequences from mutant larvae were compared to the FlyBase sequences for *l(2)not* and *tid*.

Grnd antibodies

For generating monoclonal antibodies against the extracellular domain of Grnd a peptide with the sequence ANGESRDCHGTICHPVNEFCYVATERCHPCIEVCNN QTHNYDAFLCAKECSAYKTFEPLKAEMLDIQNTQQ, corresponding to amino acids 28-98 of Grnd was fused to the N-terminus of His-MBP and used to inoculate mice. The resulting hybridoma candidates were screened for IHC and Western Blot reactivity. Grnd antibodies 7D9 and 6F10 were selected for IHC and Western Blot detection respectively.

Immunofluorescence and microscopy

Larval imaginal discs were dissected in PBS, and fixed for 20 minutes in 4% PFA. After rinsing in PBS, samples were blocked for one hour in PBT^{3} containing 5%NGS (Gibco) and 1%BSA (Gibco). Primary and secondary staining was done overnight in block at 4ºC. The primary antibodies and dilutions are listed in the **Key Resources Table**.

Secondary fluorophore-conjugated antibodies (Molecular Probes) were used at 1:250. Confocal images were obtained on either a Leica TCS SP2 Scanning confocal microscope or a Zeiss LSM 700 confocal microscope. For every experiment at least ten discs were imaged, and representative images for each experiment were chosen. Images were processed in either Adobe Photoshop CC or Fiji (Schindelin et al., 2012).

Cell counts and pupal volume measurements

WT, *alg3, dlg* and *wts* imaginal discs containing either ubiquitously expressed GFP or RFP were collected and transferred to a polystyrene tube containing 500µl of 9x Trypsin-EDTA (Sigma), 1x PBS and 0.5µg/ml Hoechst 3334. At least 20 discs per genotype were collected, and counting experiments were repeated at least five times. After ~4hrs of nutation at room temperature, proper cell dissociation was confirmed using light microscopy. Cells were counted on a hemocytometer, and by pairing off GFP and RFP positive genotypes, cell number ratios compared to WT were calculated. For the assessment of pupal sizes, larvae were staged and numbers were controlled to prevent crowding. At least 60 pupae per genotype were collected and imaged using a Leica Z16 APO microscope. Pupal length (L) and width (W) were measured using Fiji (Schindelin et al., 2012), and used to calculate pupal volume with the formula $4/3\pi(\frac{L}{2})(\frac{W}{2})^2$.

Western blotting and PNGase assay

For Western blots, larvae were dissected in PBS, using carcasses (15 larva per sample) without guts and fat body, or just the imaginal discs (60 discs per sample). Cell lysates were homogenized in 1X RIPA with protease inhibitors (Roche). 40 µg of lysate was loaded into wells. Proteins were electrophoresed at 200V for 45 minutes and blotted at 100V for 20-60 minutes depending on protein size. Membranes were blocked for an hour in 5% NFDM. For staining, the primary antibodies and dilutions are listed in the **Key Resources Table**. HRP-conjugated secondary antibodies were used at 1:10,000. Blot was developed with standard ECL reagents (Advansta). The protein de-glycosylation assay was done using PNGaseF (NEB) according to the user suggested guidelines. Each Western Blot experiment has been repeated at least three times.

Co-Culture experiments

Dissected larval fat bodies expressing Venus-tagged Egr (R4>EgrVenus) were cultured in a small volume of Schneider's medium (Gibco) containing 10% FBS (Gibco) and 1% Pen/Strep (Caisson Labs) for 3 hours at 29°C. At least 12 larval imaginal discs of the genotype of interest were added to this mixture and co-cultured for 5 hours at 29°C. After culturing the discs are rinsed in PBS, and fixed for 20 minutes in 4% PFA. Each Co-Culture experiment has been repeated at least three times.

★Quantification and Statistical Analysis

Fiji (Schindelin et al., 2012) was used to collect pupal dimensions, fluorescence intensity, Western Blot quantification and disc/clone size measurements. Graphpad Prism 5.03 and Excel (Microsoft Office) were used for statistical analysis and graphical representations. Column graphs show the mean with error bars indicating standard

deviation, unless indicated otherwise. All experiments were repeated at least three times. Specific n value per experiment indicated in the method details section. The Student's t-test was used to determine statistical significance, as well as the F-test for determining the equality of variances in two-sample comparisons.

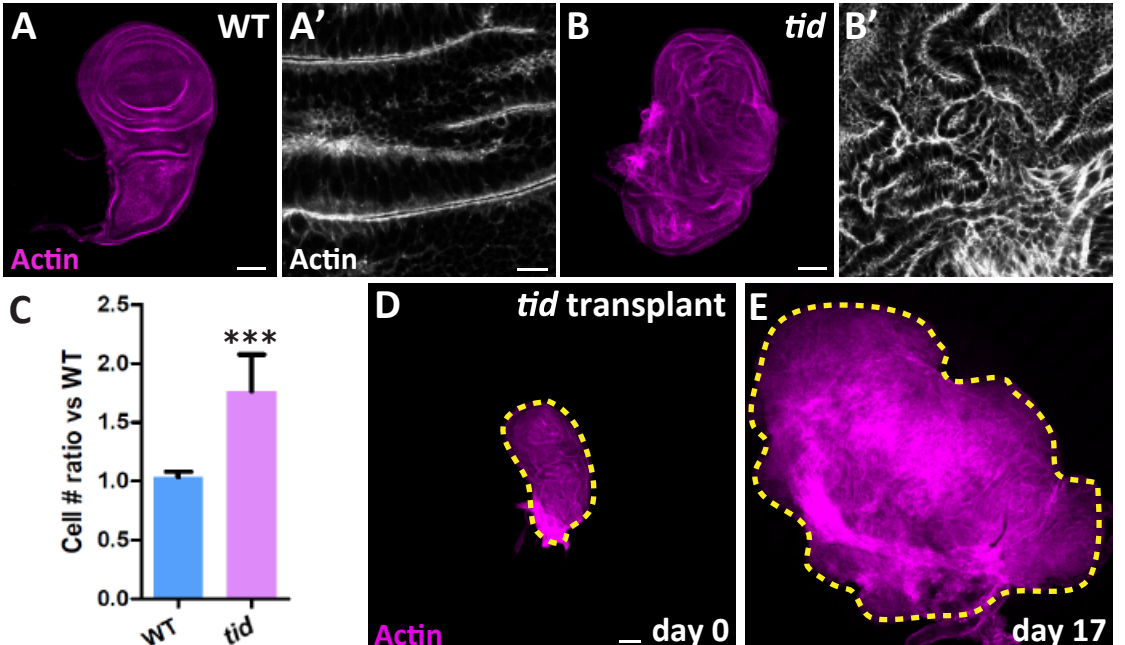
A
WT
Actin
A'
Actin
B
tid
B'
C
Cell # ratio vs WT
2.5
2.0
1.5
1.0
0.5
0.0
***
WT
tid
D
tid transplant
Actin
day 0
E
day 17

Figure 1

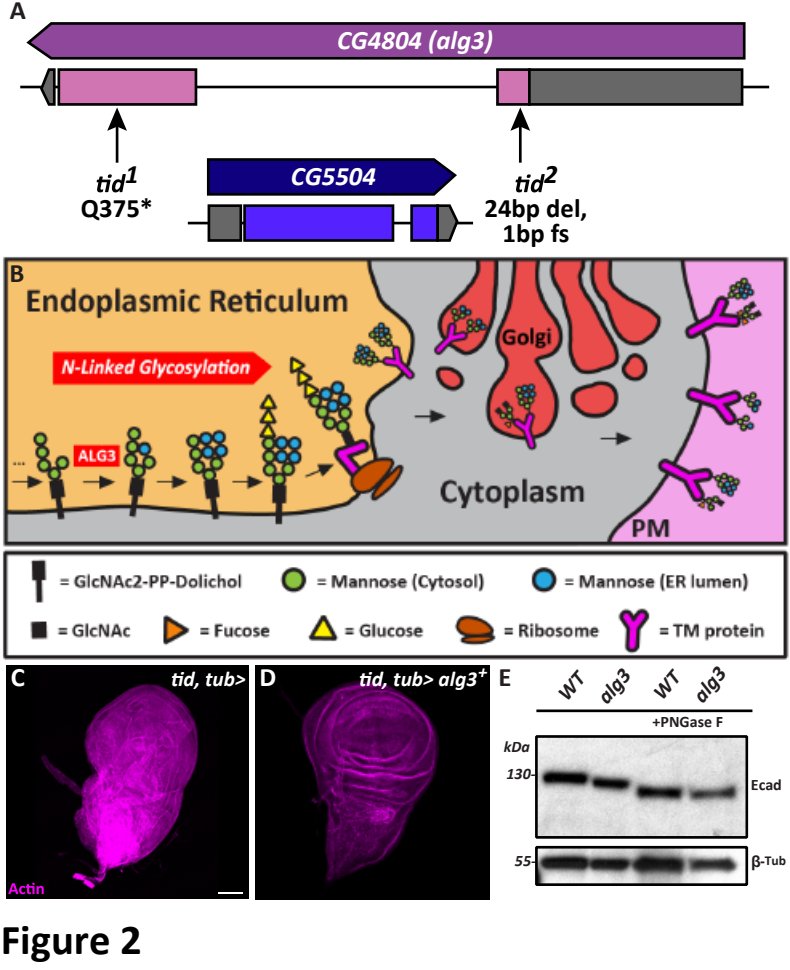
A
CG4804 (alg3)
tid1
Q375*
CG5504
tid2
24bp del,
1bp fs
B
Endoplasmic Reticulum
N-Linked Glycosylation
ALG3
Golgi
Cytoplasm
PM
= GlcNAc2-PP-Dolichol
= Mannose (Cytosol)
= Mannose (ER lumen)
= GlcNAc
= Fucose
= Glucose
= Ribosome
= TM protein
C
tid, tub>
Actin
D
tid, tub> alg3+
E
WT
alg3
WT
alg3
+PNGase F
kDa
130-
Ecad
55-
β-Tub

Figure 2

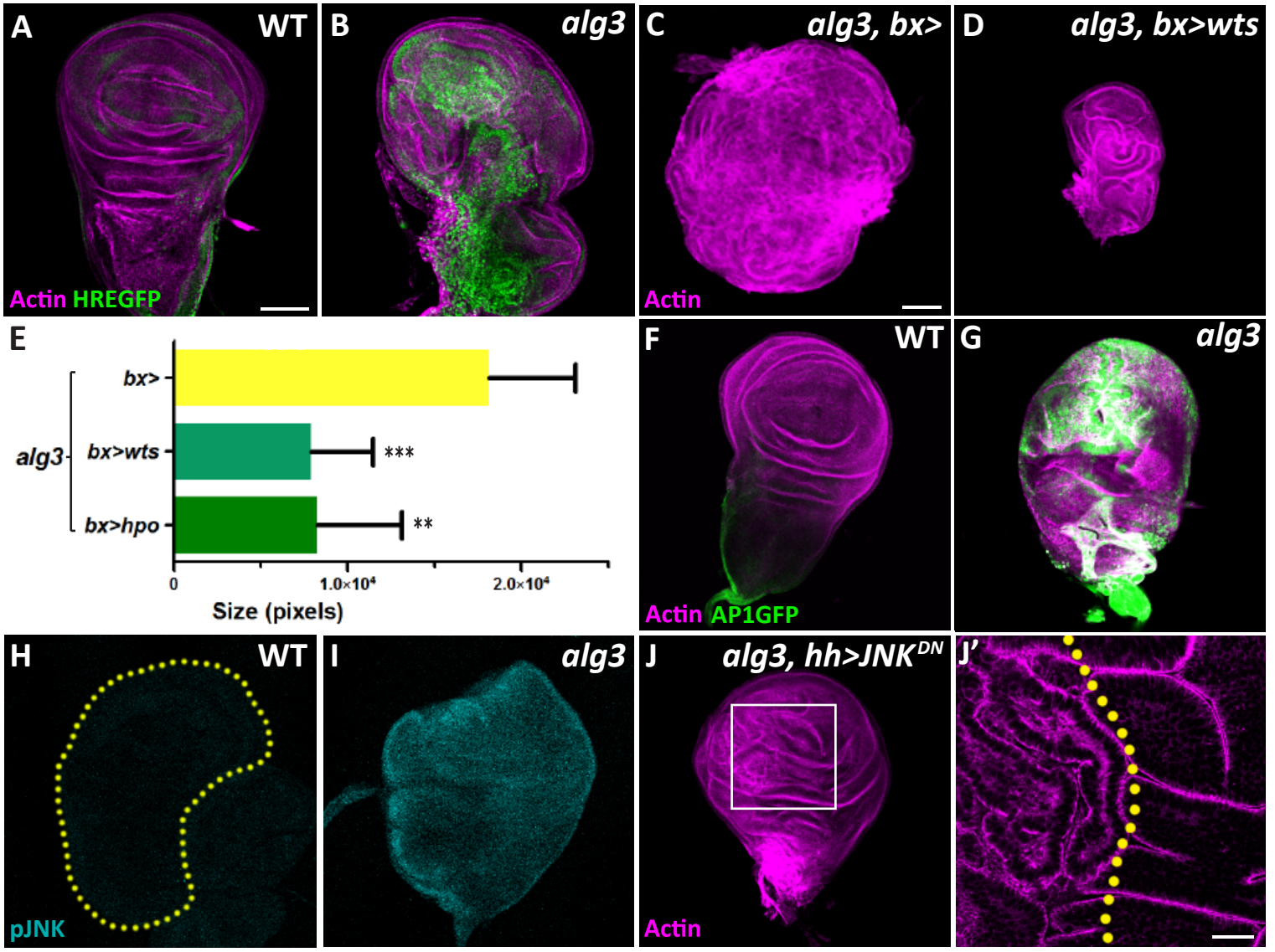
A
WT
Actin HREGFP
B
alg3
C
alg3, bx>
Actin
D
alg3, bx>wts
E
bx>
alg3
bx>wts
bx>hpo
***
**
0
1.0×10⁴
2.0×10⁴
Size (pixels)
F
WT
Actin AP1GFP
G
alg3
H
WT
pJNK
I
alg3
J
alg3, hh>JNK^DN
Actin
J'

Figure 3

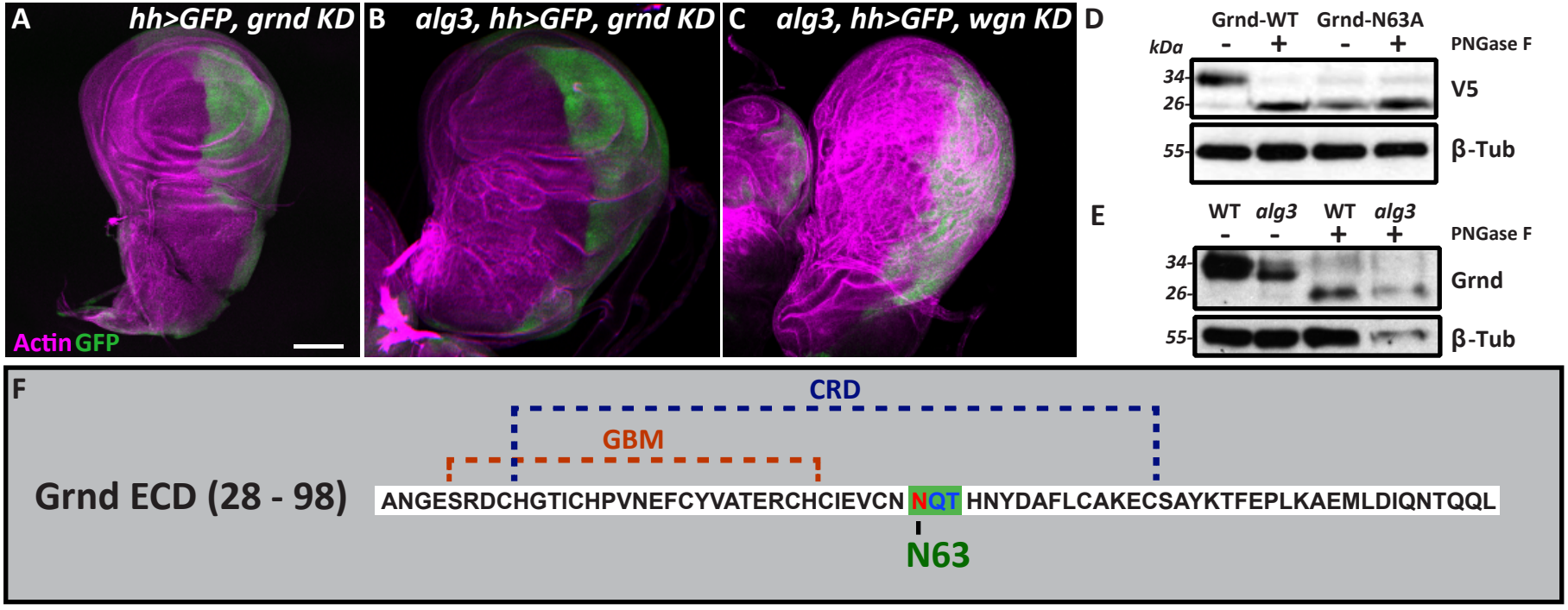
A
hh>GFP, grnd KD
Actin GFP
B
alg3, hh>GFP, grnd KD
C
alg3, hh>GFP, wgn KD
D
Grnd-WT
Grnd-N63A
kDa
-
+
-
+
PNGase F
34
26
V5
55
β-Tub
E
WT
alg3
WT
alg3
-
-
+
+
PNGase F
34
26
Grnd
55
β-Tub
F
CRD
GBM
Grnd ECD (28 - 98)
ANGESRDCHGTICHPVNEFCYVATERCHCIEVCN NQT HNYDAFLCAKECSAYKTFEPLKAEMLDIQNTQQL
N63

Figure 4

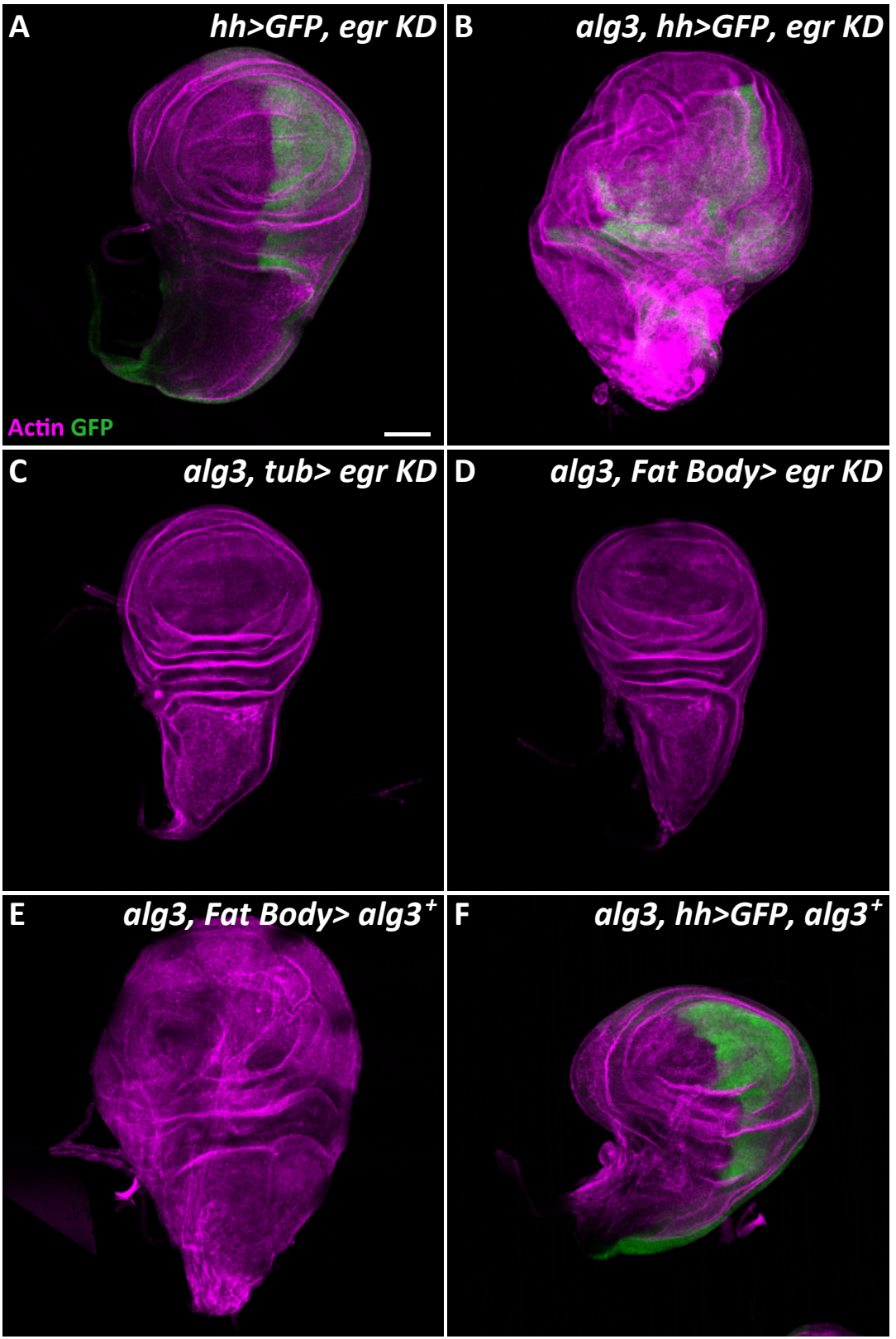
A
hh>GFP, egr KD
B
alg3, hh>GFP, egr KD
Actin GFP
C
alg3, tub> egr KD
D
alg3, Fat Body> egr KD
E
alg3, Fat Body> alg3+
F
alg3, hh>GFP, alg3+

Figure 5

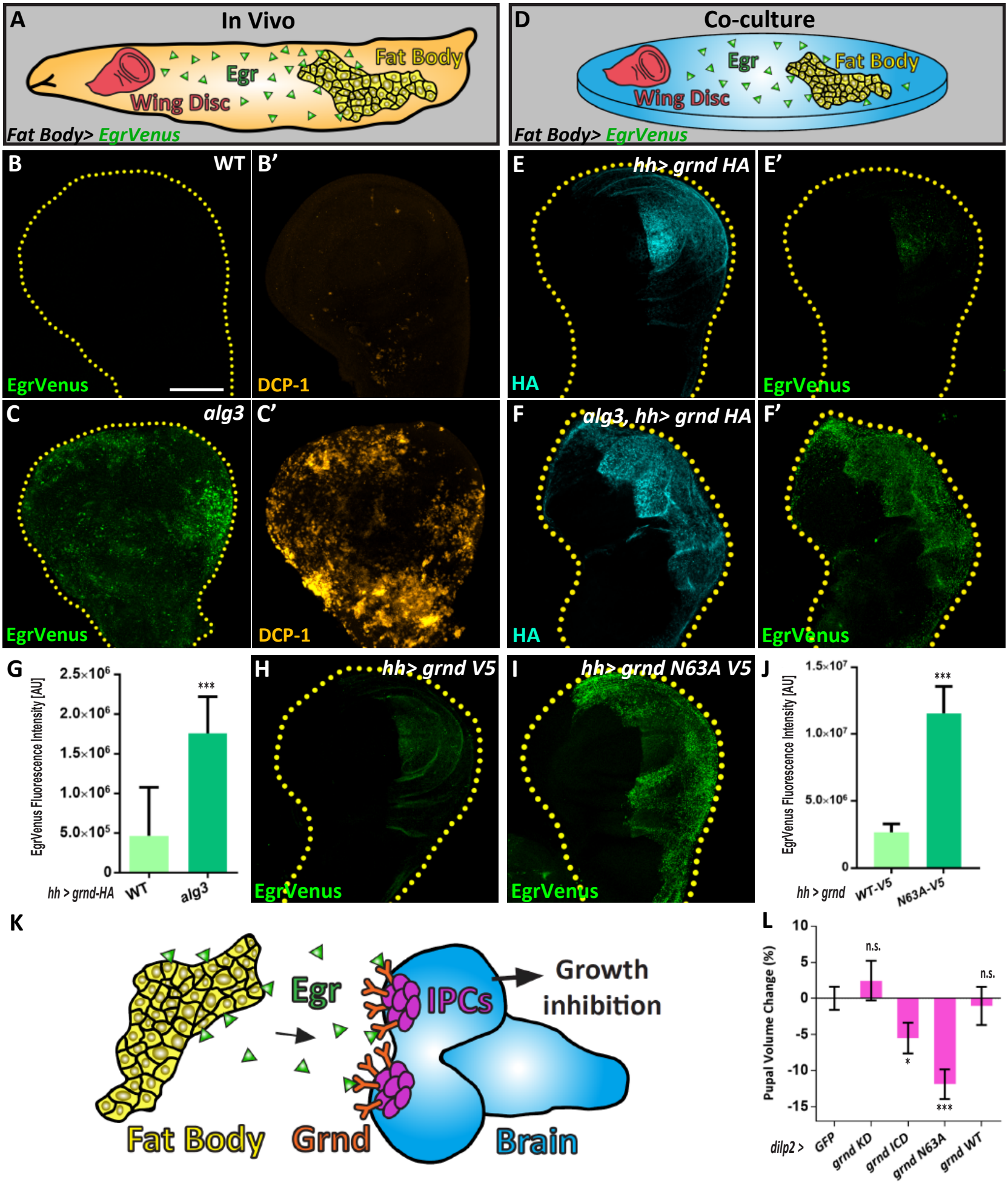
A
In Vivo
Egr
Fat Body
Wing Disc
Fat Body> EgrVenus
D
Co-culture
Egr
Fat Body
Wing Disc
Fat Body> EgrVenus
B
WT
EgrVenus
B'
DCP-1
E
hh> grnd HA
HA
E'
EgrVenus
C
alg3
EgrVenus
C'
DCP-1
F
alg3, hh> grnd HA
HA
F'
EgrVenus
G
EgrVenus Fluorescence Intensity [AU]
2.5×10^6
2.0×10^6
1.5×10^6
1.0×10^6
5.0×10^5
0
***
hh > grnd-HA
WT
alg3
H
hh> grnd V5
EgrVenus
I
hh> grnd N63A V5
EgrVenus
J
EgrVenus Fluorescence Intensity [AU]
1.5×10^7
1.0×10^7
5.0×10^6
0
***
hh > grnd
WT-V5
N63A-V5
K
Egr
IPCs
Growth inhibition
Fat Body
Grnd
Brain
L
Pupal Volume Change (%)
10
5
0
-5
-10
-15
n.s.
*
***
n.s.
dilp2 >
GFP
grnd KD
grnd ICD
grnd N63A
grnd WT

Figure 6

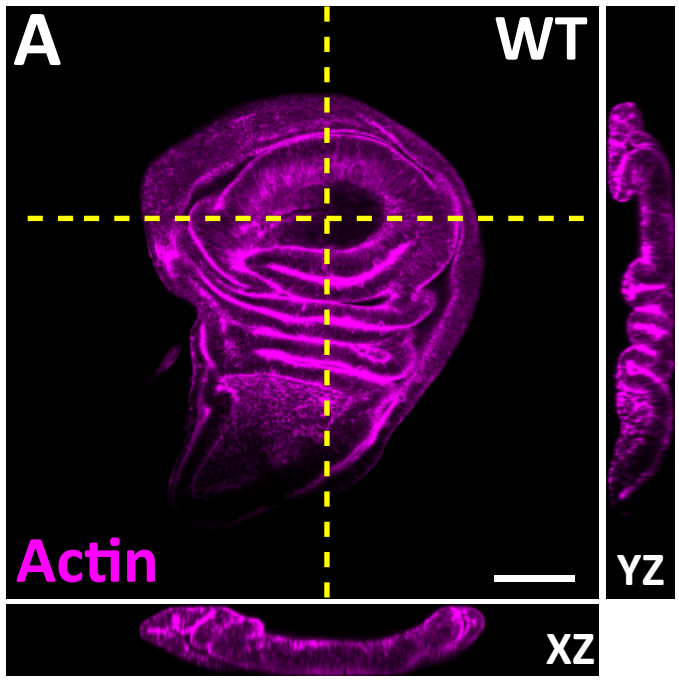

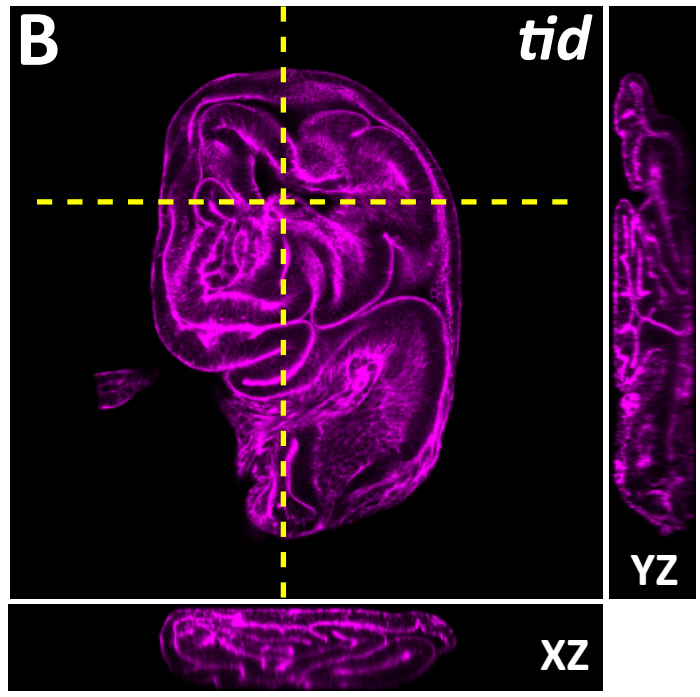

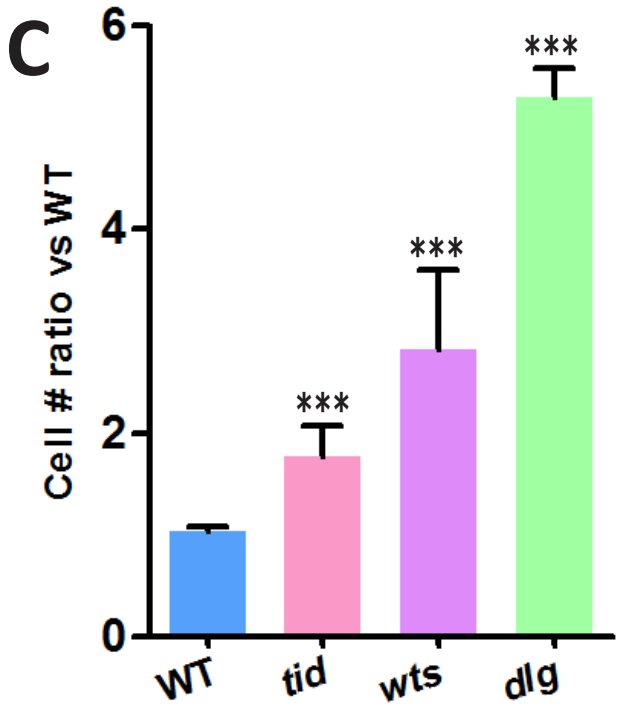

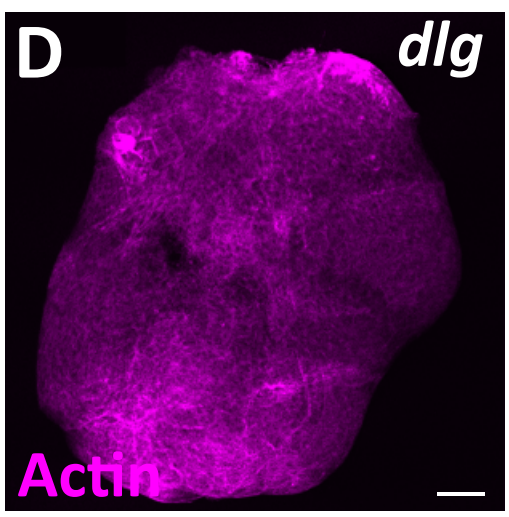

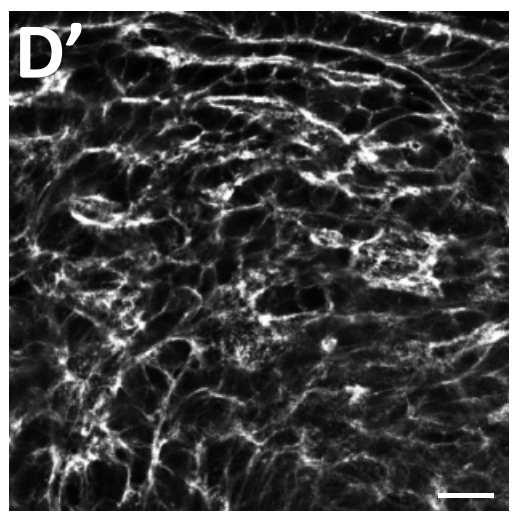

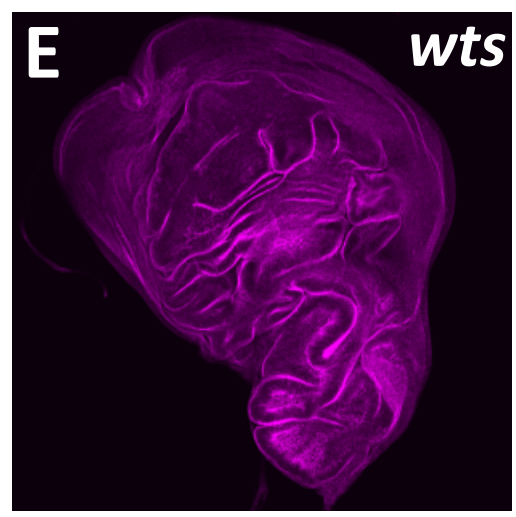

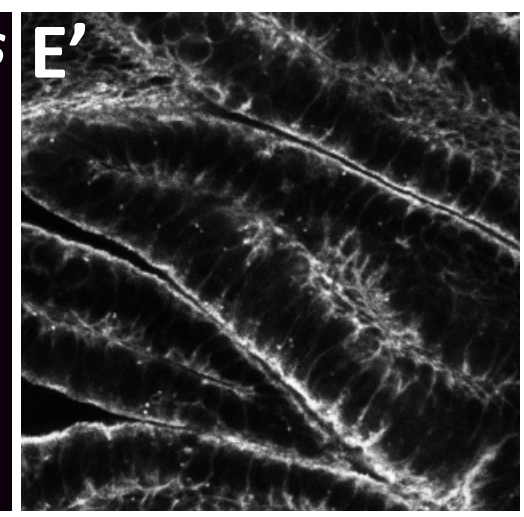

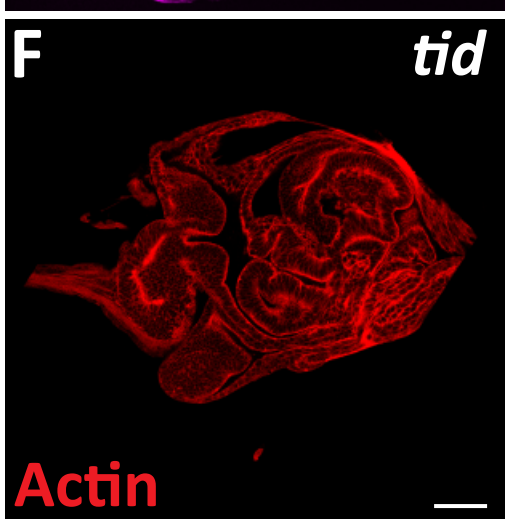

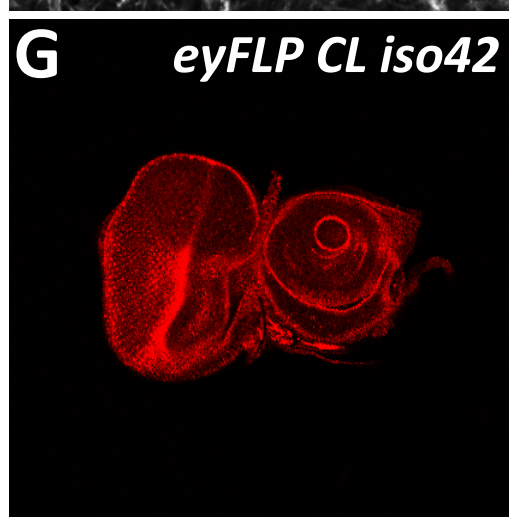

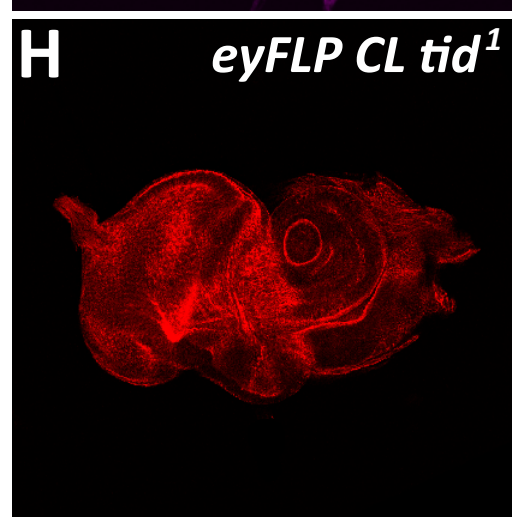

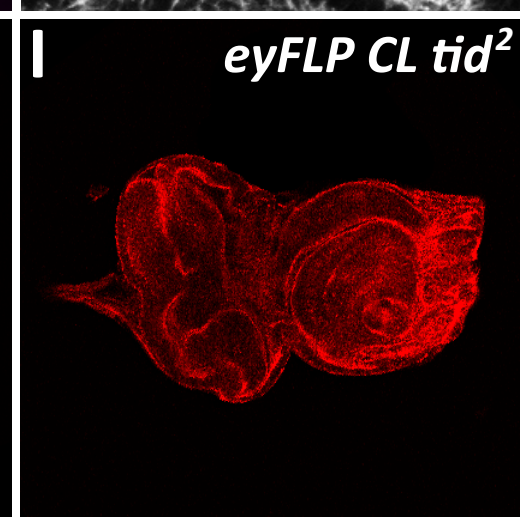

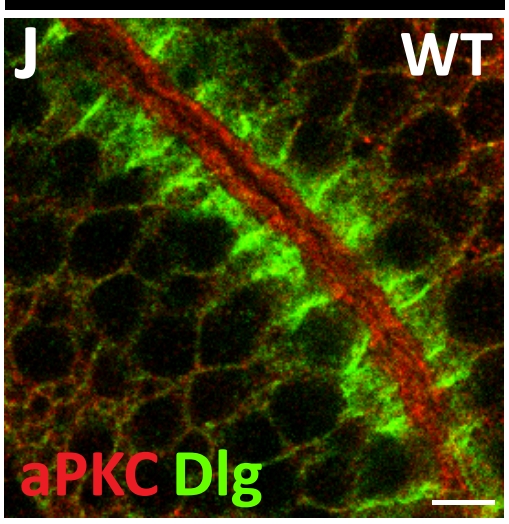

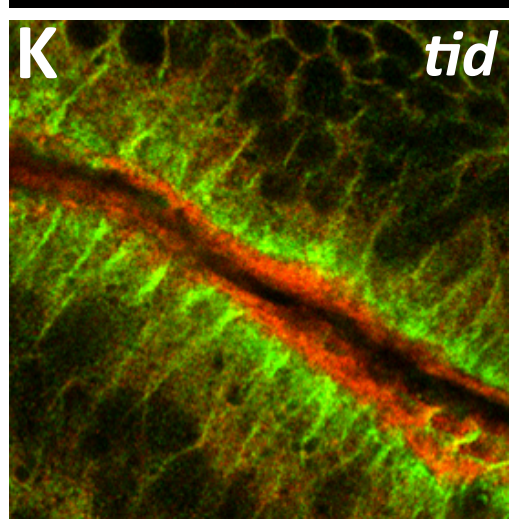

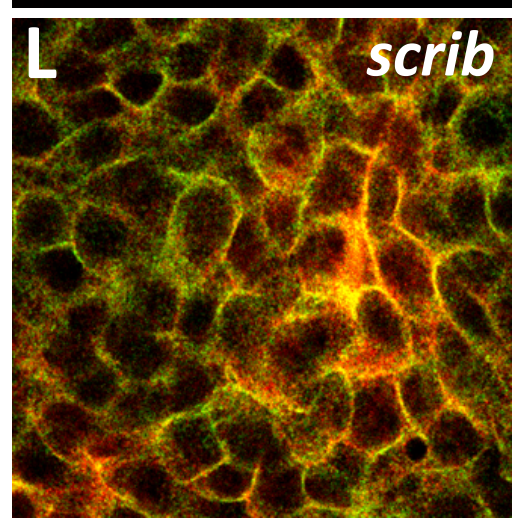

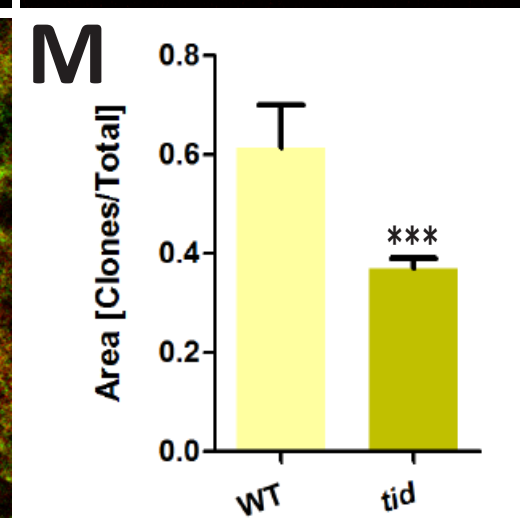

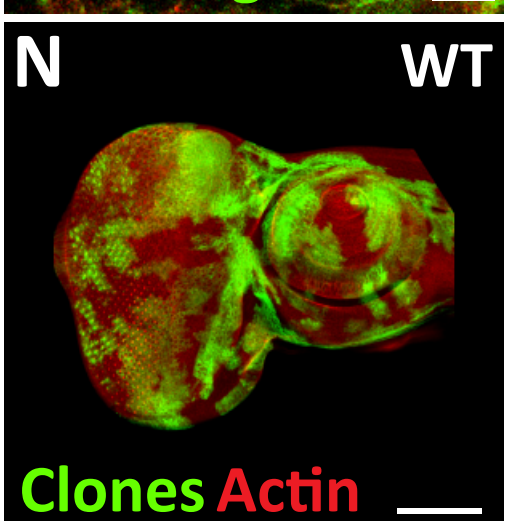

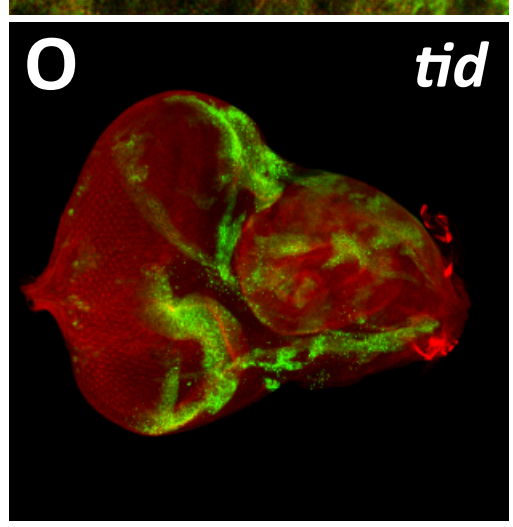

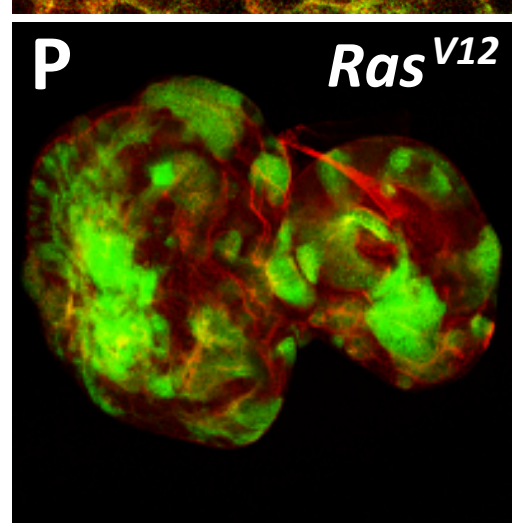

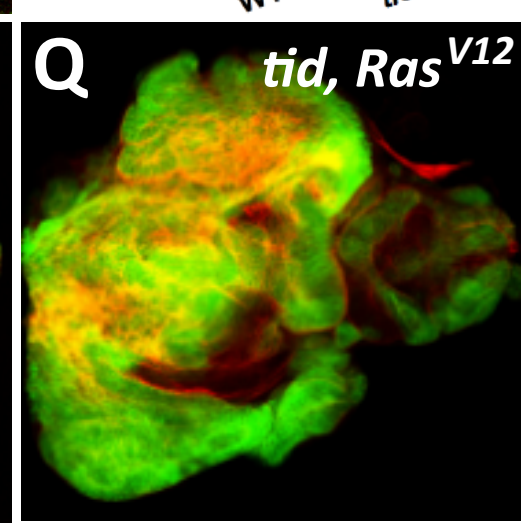

Supplementary Figure 1

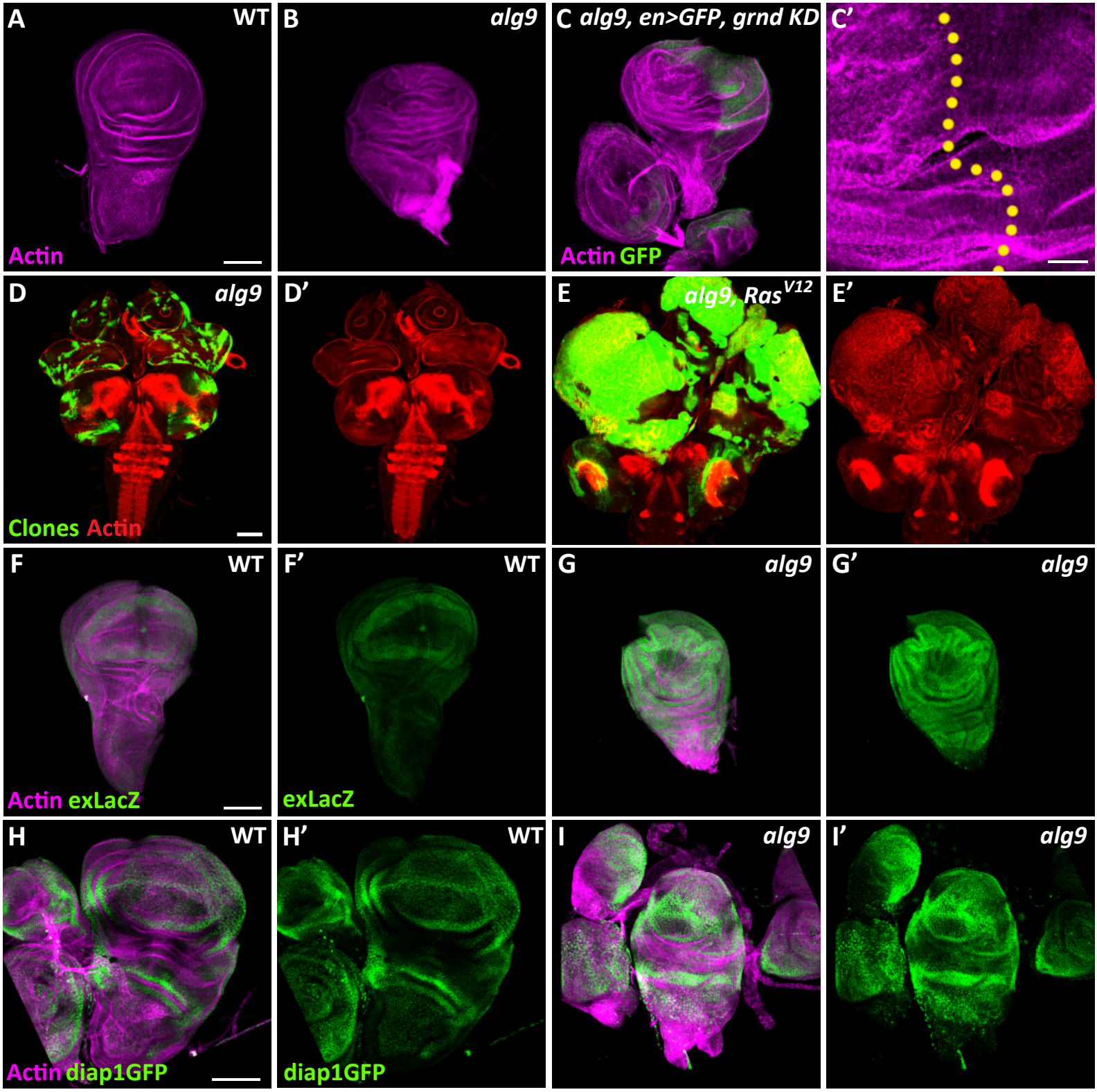

Supplementary Figure 2

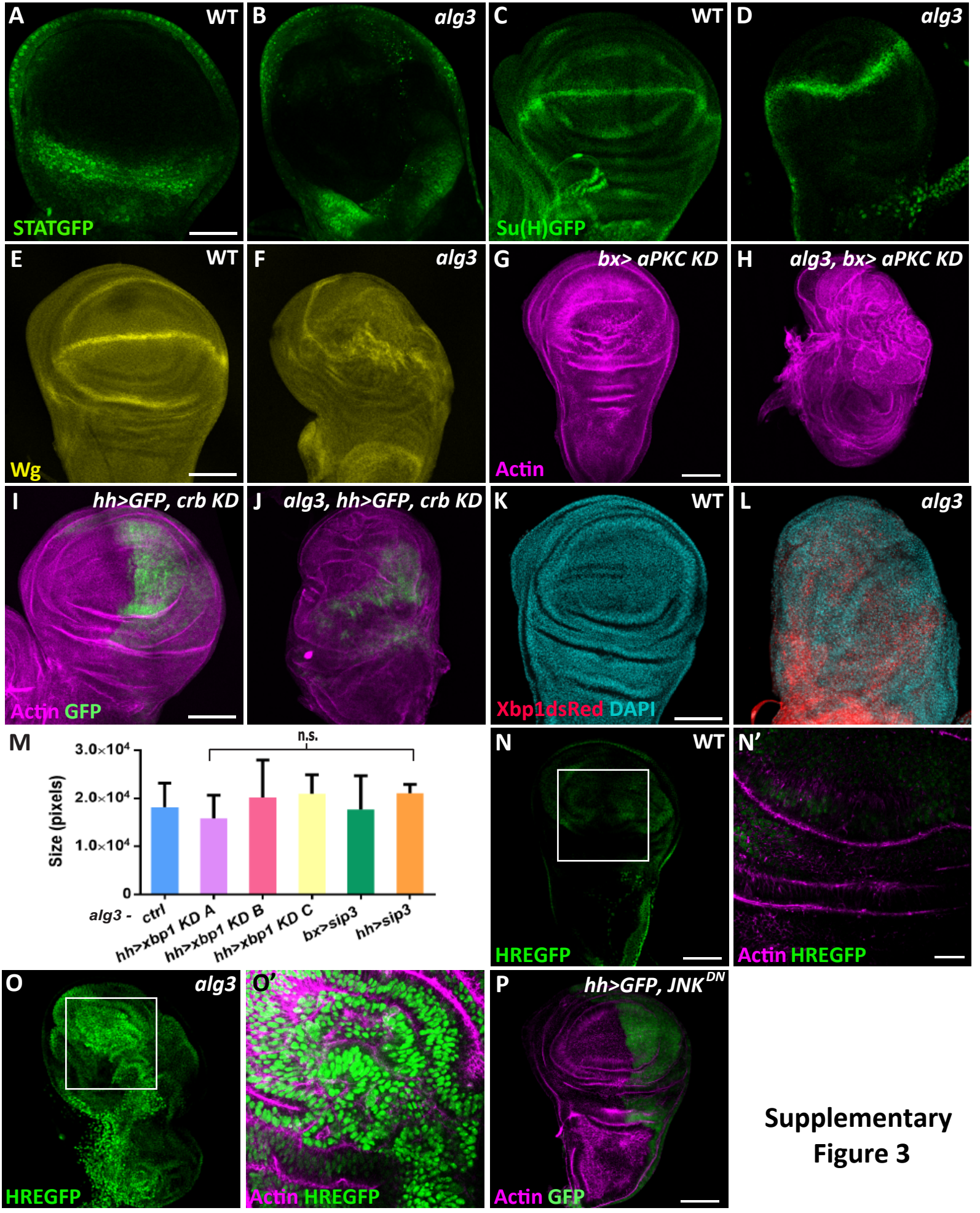

Supplementary Figure 3

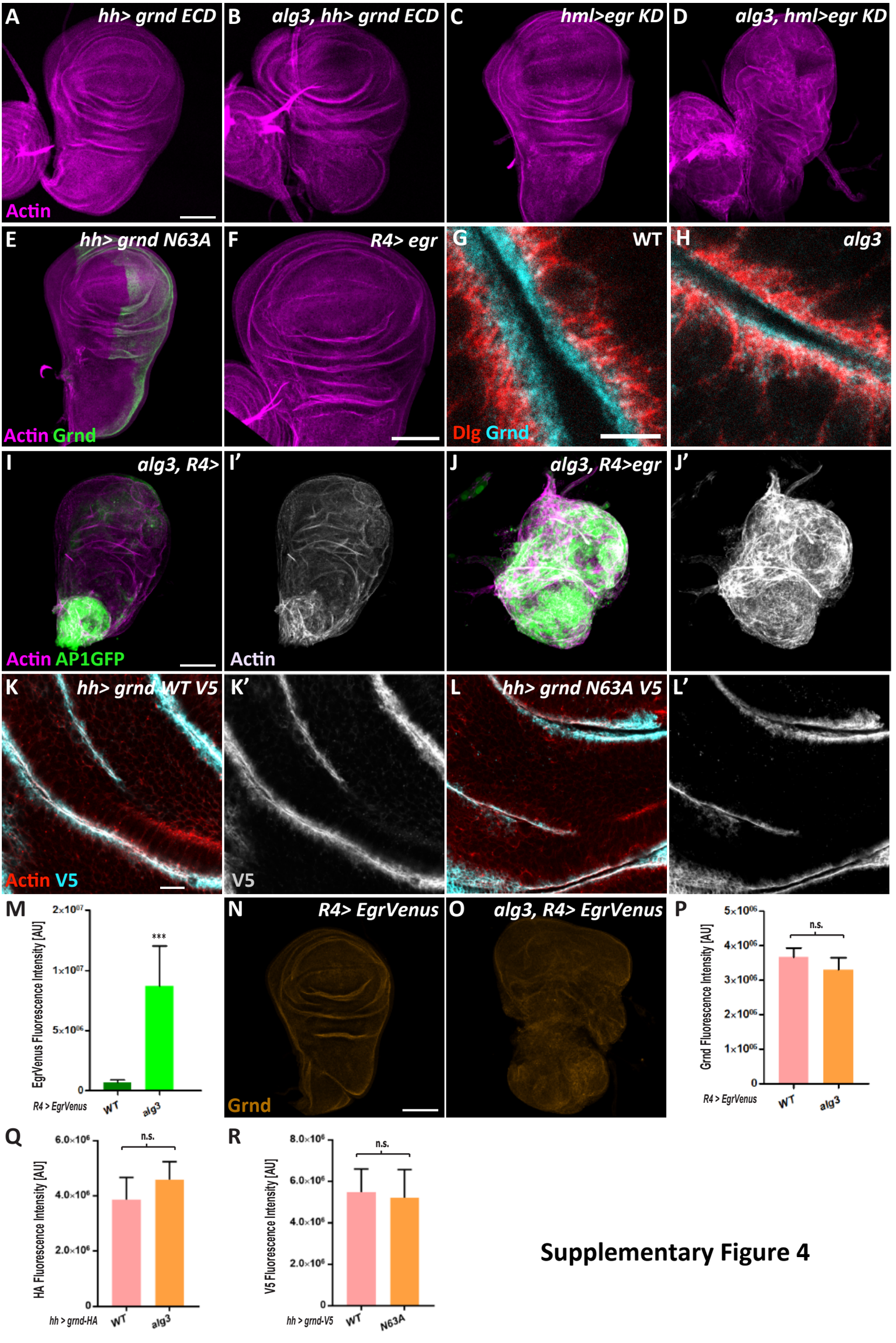

Supplementary Figure 4